

Stable Deuterium-Tritium burning plasmas with improved confinement in the presence of energetic-ion instabilities.

Authors

Jeronimo Garcia^{1*}, Yevgen Kazakov², Rui Coelho³, Mykola Dreval⁴, Elena de la Luna⁵, Emilia R. Solano⁵, Ziga Stancar⁶, Jacobo Varela⁷, Matteo Baruzzo⁸, Emily Belli⁹, Phillip J. Bonfiglio¹⁰, Jeff Candy⁹, Costanza F. Maggi⁶, Joelle Mailloux⁶, Samuele Mazzi¹, Jef Ongena², Michal Poradzinski⁶, Juan R. Ruiz¹¹, Sergei Sharapov⁶, David Zarzoso¹² and JET contributors^a

Affiliations

¹CEA, IRFM, F-13108 Saint-Paul-lez-Durance, France.

²Laboratory for Plasma Physics, LPP-ERM/KMS, EUROfusion Consortium member, TEC Partner, Brussels, Belgium.

³Instituto de Plasmas e Fusao Nuclear, Instituto Superior Técnico, Universidade de Lisboa, Portugal.

⁴National Science Center Kharkiv Institute of Physics and Technology, 1 Akademichna Str., Kharkiv 61108, Ukraine.

⁵Laboratorio Nacional de Fusion, CIEMAT, 28040 Madrid, Spain.

⁶United Kingdom Atomic Energy Authority, Culham Science Centre, Abingdon, Oxon OX14 3DB, United Kingdom of Great Britain and Northern Ireland.

⁷Universidad Carlos III de Madrid, 28911 Leganes, Madrid, Spain.

⁸Dip.to Fusione e Tecnologie per la Sicurezza Nucleare, ENEA C. R. Frascati, via E. Fermi 45, 00044 Frascati (Roma), Italy.

⁹General Atomics, PO Box 85608, San Diego, CA 92186-5608, United States of America.

¹⁰Princeton Plasma Physics Laboratory, Princeton, New Jersey 08534, USA.

¹¹Rudolf Peierls Centre for Theoretical Physics, University of Oxford, Oxford OX1 3NP, United Kingdom.

¹²Aix-Marseille Université, CNRS, Centrale Marseille, M2P2, UMR 7340 Marseille, France.

^a See the author list of “Overview of T and D-T results in JET with ITER-like wall” by CF Maggi et al. to be published in Nuclear Fusion Special Issue: Overview and Summary Papers from the 29th Fusion Energy Conference (London, UK, 16-21 October 2023)

Abstract

Providing stable and clean energy sources is a necessity for the increasing demands of humanity. Energy produced by fusion reactions, in particular in tokamaks, is a promising path towards that goal. However, there is little experience with plasmas under conditions close to those expected in future fusion reactors, because it requires the fusion of Deuterium (D) and Tritium (T), while most of the experiments are currently performed in pure D. After more than

20 years, the Joint European Torus (JET) has carried out new D-T experiments with the aim of exploring the unique characteristics of burning D-T plasmas, such as the presence of highly energetic ions. A new stable, high confinement and impurity-free D-T regime, with strong reduction of energy losses with respect to D, has been found. Multiscale physics mechanisms critically determine the thermal confinement and the fusion power yield. These crucial achievements importantly contribute to the establishment of fusion energy generation as an alternative to fossil fuels.

Corresponding author email: jeronimo.garcia@cea.fr

Introduction

Modern societies are eager to increase their energy resources, which currently are largely provided by fossil fuels. In this context, plasmas, i.e. the fourth state of matter, which are characterized by the presence of free charged particles, can provide a carbon-free energy source through fusion reactions of light atom nuclei. For that purpose, plasmas must be well confined and reach high pressure in order to overcome the electrostatic repulsion of particles. Magnetic containment is one of the most promising routes towards this goal. The tokamak concept, in which plasmas are confined both by a high toroidal electric current, I_p , and a toroidal magnetic field, B_T , is particularly promising. Tokamaks have made great progress from their initial proposal [1] [2]. Plasmas with good thermal confinement have been achieved in high-performance tokamak discharges when turbulence-driven energy losses (one of the main physics mechanisms by which plasmas lose their thermal confinement) are strongly reduced. This is the case for the H-modes [3] or internal transport barrier (ITB) regimes [4], in which steep pressure gradients are formed, leading to high plasma pressure. Recently, the EAST [5] and KSTAR [6] tokamaks have reported significant advances. Long-sustained high-performance plasmas were obtained in conditions of low turbulent heat transport with simultaneous avoidance of dangerous magnetohydrodynamic (MHD) bursts, called edge localized modes (ELMs) [7], which are characteristic of H-modes. Such bursts can lead to rapid expulsion of edge plasma and hence to high levels of heat and particle flux to the tokamak wall.

On the one hand, these advances have clarified the route towards a potential fusion energy commercial reactor. On the other hand, the results obtained are not enough to provide a clear insight into how future energy-producing reactor plasmas are expected to behave. The reason is that in significant contrast to plasmas produced nowadays, formed almost exclusively by pure Deuterium (D), energy-producing plasmas will use Deuterium and Tritium (T) to produce 14.1 MeV neutrons and 3.5 MeV ^4He nuclei (alpha particles). The presence of T has been identified as a potential source of significant changes with respect to pure D plasmas, particularly in terms of turbulence or MHD characteristics [8] [9]. Furthermore, the presence of a small and yet very energetic population of alpha particles, which will provide the main self-heating mechanism through collisions to the thermal plasma, leads to conditions that are mostly unexplored and have been identified as potentially detrimental. The highly energetic fusion-born alpha particles mainly transfer energy to electrons (rather than to thermal ions) by collisions, thus providing strong electron heating. Conditions in which the electron temperature, T_e , is significantly higher than the ion temperature, T_i , have been identified as leading to unfavorable destabilization of turbulence and clamping of the ion temperatures at very low values, as shown in plasmas with pure electron heating by means of electromagnetic waves [10] [5]. Moreover, alpha particles do not provide significant torque and therefore lead to low toroidal rotation, reducing rotation-driven suppression of turbulence [11][12]. Finally, they can resonantly destabilize Alfvén waves that can produce stochastic transport of alpha particles and hence reduction of fusion energy generation [13][14][15][16].

These novel characteristics are in contrast to present-day experiments which are typically heated by neutral beam injection (NBI) at energies ~ 100 keV. NBI dominantly heats ions, not electrons, and provides significant torque. Unlike fusion-generated alpha particles, they produce a sizeable fast-ion density fraction with $T_i/T_e > 1$. In such conditions, it is well known that high confinement can be obtained [6].

The Joint European Torus (JET) tokamak [17], which is the only tokamak in the world capable of operating with T, has undergone a new experimental campaign in D-T, DTE2 [18], with the aim of providing solid evidence on the characteristics of D-T plasmas. A world record of fusion energy was produced in JET at the end of 2021

[19] by developing H-mode plasmas with ELMs. However, such an impressive result was obtained under conditions of high NBI power. In this paper, we describe DTE2 plasmas that, rather than maximizing the production of fusion energy, aim to capture other important characteristics expected in future fusion reactors, such as the simultaneous development of conditions with dominant total heating fraction transferred to the electrons, low input torque, and the triggering of Alfvén wave instabilities. These characteristics were not studied in the DTE2 fusion energy record, nor in the first D-T campaign in JET (DTE1)[9] or TFTR[8] in the 90s, since in both cases the maximization of the fusion power by using high NBI power was mostly explored and in such conditions plasmas with $T_i/T_e > 1$ and high ion heating and rotation are obtained. Therefore, the study presented in this paper represents the first time that this path has been pursued in D-T plasmas.

We show that very good properties are achieved in terms of energy confinement and stability. The type of confinement expected in baseline reactor plasmas is obtained because of the better energy confinement in D-T with respect to the same conditions in D. In particular, for the electrons, energy losses by transport are low, which allows temperatures of about 110 million K. For the ions, the core heat transport is significantly reduced in D-T compared to D when instabilities generated by the energetic ions are observed. Under these conditions, up to 1 MW of fusion power is generated with only 2.4 MW of external ion heating. This type of plasma provides an integrated solution for future tokamak reactors, since, despite developing an H-mode, deleterious ELMs are avoided. The results indicate improved energy confinement in D-T burning plasma conditions.

D-T plasmas development and comparison to D

Several plasma configurations and D-T concentrations were explored in JET to cover a wide range of possible configurations in future tokamak reactors. To minimize the external torque and hence the toroidal rotation, the plasmas presented in this study were mostly heated with electromagnetic waves resonating at the ion cyclotron frequency (ICRF), which ensures that a low external torque is applied. ICRF heating can accelerate ions to MeV energies and in these plasmas 1% of H was used as a minority wave resonator. Additional lower heating power levels of NBI were used with the aim of reaching high temperatures. The discharge #99896, shown in Fig. 1A represents the type of plasma performed. The chosen D-T concentration was $\sim 50\%D - 50\%T$ as it is expected to deliver the maximum fusion power in future tokamak fusion reactors.

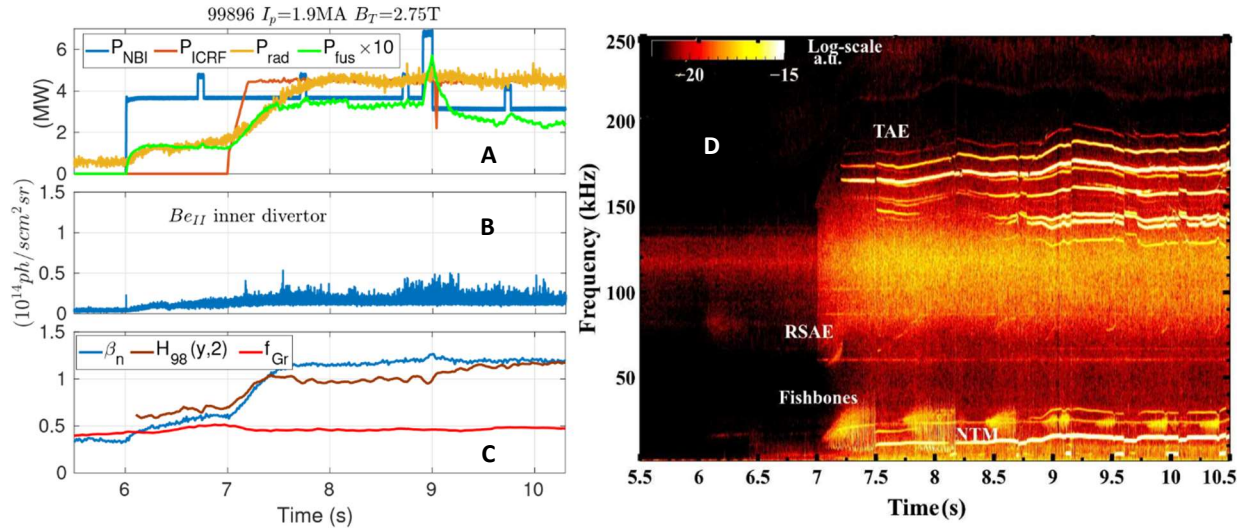


Fig. 1. Main characteristics of the D-T discharge #99896. (A) Time evolution of discharge #99896, with toroidal current $I_p = 1.9$ MA, magnetic field $B_T = 2.75$ T, and $q_{95} = 4.5$, heated mainly with ICRF power, $P_{ICRF} = 4.5$ MW. The NBI power, $P_{NBI} \sim 3.5$ MW, was also injected with deuterium beams, before 9 s, and tritium beams, after 9 s. The radiated power, P_{rad} represents 60% of the total input power. The fusion power obtained reaches a maximum of $P_{fus} \sim 0.5$ MW. (B) Time evolution of edge fluctuations as obtained from the Be_{II} line emission from the inner divertor. (C) Time evolution of β_N , defined as $\beta_N = \beta a B_T / I_p$ [%] with β the ratio between magnetic and thermal

pressure and a the plasma minor radius, $H_{98}(y,2)$ and $f_{Gr} = \bar{n}_e/n_{Gr}$ the Greenwald fraction with \bar{n}_e the average density and n_{Gr} the Greenwald density defined as $n_{Gr} = I_p/\pi a^2$. (D) Time evolution of magnetic perturbations detected by the Mirnov coils.

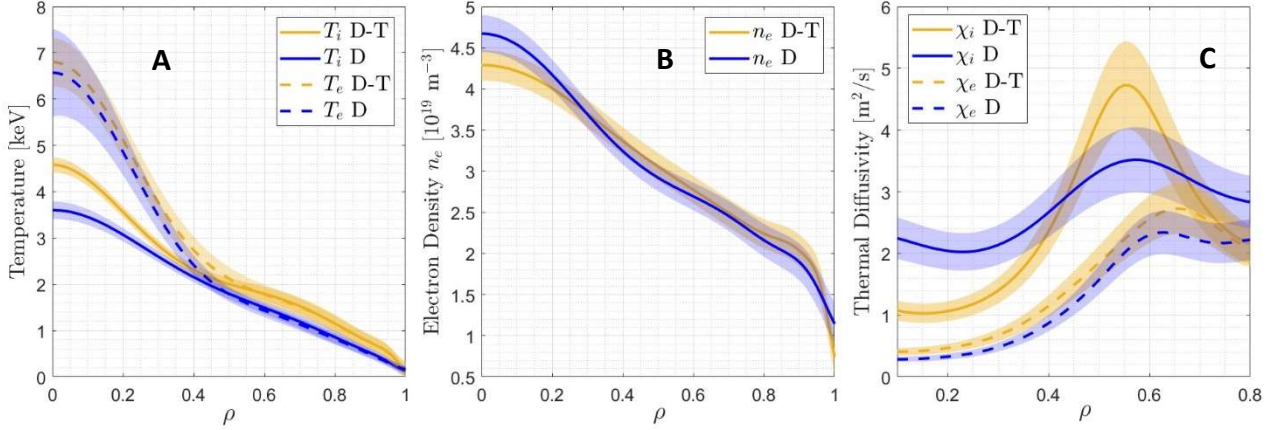


Fig. 2. Comparison between the D-T discharge #99896 and the D counterpart #100871. (A) Comparison between T_i and T_e for the D-T discharge #99896 and the D counterpart #100871. T_i is measured by the charge-exchange technique on impurity ions. T_e is obtained by means of LIDAR and high-resolution Thomson scattering (HRTS). An average over 8.5 s–8.7 s is performed. ρ is defined as the square root of the normalized toroidal magnetic flux. (B) Comparison between electron density, n_e , for the D-T discharge #99896 and the D counterpart #100871. n_e is measured with HRTS. (C) Comparison between χ_i and χ_e obtained by power balance analysis for the D-T discharge #99896 and the D counterpart #100871.

During the phase with ICRF and NBI heating, the thermal confinement time of this plasma, τ , calculated excluding the contribution of energetic ions, is the reference in the ITER baseline conditions as $H_{98}(y,2) = \tau/\tau_{IPB98} \geq 1$ (Fig.1C) with τ_{IPB98} the energy confinement time predicted by the IPB98(y,2) scaling (20). This result is obtained under low rotation conditions, since the Mach number at $\rho = 0.5$, $M = v_{tor}/c_s \sim 0.15$, with v_{tor} the plasma rotation, $c_s = \sqrt{T_e/m_i}$ the sound speed and m_i the Deuterium ion mass, is lower than that expected in ITER D-T plasmas (21).

As shown in Fig.1B these results are obtained in the presence of small edge fluctuations rather than ELMs with $\beta_N = 1.2$ and $f_{Gr} \sim 0.45$ (Fig.1C). Analysis using the TRANSP suite of modeling codes (22) indicates that 56% of the total auxiliary heating is transferred to electrons. The high electron heating is confirmed by the observation that $T_e > T_i$, notably in the region $\rho < 0.4$ with $T_e/T_i \sim 1.4$ on the magnetic axis. On the contrary, during the NBI only phase, $H_{98}(y,2) = 0.7$, indicating a lower confinement compared to the phase with injected ICRF heating. In terms of fusion power, $P_{fus} \sim 0.5$ MW was obtained. Finally, the radiated power reaches 60% of the total power injected and is located at the plasma separatrix close to the X-point, which indicates that the accumulation of core impurities, usually a concern in high confinement plasmas in a metallic wall environment such as in JET (23), is avoided.

The good thermal confinement of discharge #99896 is obtained in the presence of generally-believed deleterious electromagnetic perturbations over a wide range of frequencies when ICRF heating is added, as shown in Fig.1D. We can identify perturbations generated by the interplay between energetic ions and Alfvén waves, such as toroidal Alfvén eigenmodes (TAE) (24, 25) and reversed-shear Alfvén eigenmodes (RSAE) (26). Fishbone instabilities (27)(28) related to the interaction between energetic ions and MHD are also present. All of this activity corroborates the presence of highly energetic ions in the plasma. MHD activity and in particular neoclassical tearing modes (NTM) (29)(30) are also found.

An equivalent discharge, #100871, in terms of input power, radiated power, and density, with pure D was also carried out to compare to the characteristics of D-T discharges. The match was successful, including a similar pattern of magnetic instabilities. The comparison between the temperature and electron density profiles between D-T and D is shown in Fig.2(A and B). Although the electron density is nearly identical in D-T and D, both T_e and T_i are higher in D-T for the entire plasma radius. In particular, in the plasma core, an increase in T_i slope is obtained. Since the heating deposition profiles are very similar in D-T and D in the plasma inner core, as verified

with TRANSP, such a change in T_i could have its origin in differences in thermal transport. Indeed, a significant change is found, as demonstrated by calculating the power balance heat diffusivity for ions, χ_i , and electrons, χ_e , (see Fig. 2C). In D-T, χ_i shows a drop in the plasma core starting from $\rho = 0.4$ and reaching $\chi_{i,D-T}/\chi_{i,D} \sim 0.5$ at $\rho = 0.2$. The electron heat diffusivity, χ_e , remains very low for D-T and D, which leads to very peaked T_e , similar to ITB plasmas observed in other high electron heated plasmas such as the super I-mode developed in EAST (5). Importantly, $\chi_{i,D-T}/\chi_{e,D-T} \sim 2$ while it is doubled for pure D indicating deteriorated ion thermal confinement.

D-T density-ratio scans were performed to evaluate the impact of T on plasma characteristics. As an example, the discharge #99817 was performed in conditions similar to #99896 but with 85% T fraction and $B_T = 3.7$ T. The total heating to electrons under these conditions was 70% as obtained from TRANSP, with $P_{fus} \sim 1$ MW and T_e reaching 110 million K and T_i 60 million K with only 8 MW of input power. Similar to discharge #99896, a broad range of energetic-ion instabilities was obtained. Compared to the case with $\sim 50\%D - 50\%T$, $\chi_{i,D-T}/\chi_{e,D-T}$ is reduced to ~ 1 , which means that the presence of T in the plasma is a key player in reducing ion thermal energy losses due to heat transport.

Core instabilities analyses

Beyond large-scale MHD and Alfvén-driven fluctuations, small-scale microturbulence driven by the Ion Temperature Gradient (ITG) instability [31] is one of the major threats to plasma thermal confinement. In JET plasmas, ITG modes, destabilized at ion-gyroradius scales, ~ 1 cm, are usually responsible for enhancing core radial energy transport even in strongly electron-heated plasmas [32]. Instead, energy transport driven by instabilities at electron gyroradius scales, ~ 0.1 mm, i.e. by electron temperature gradient modes (ETG), is found to not contribute significantly to overall outward transport in the plasma core [33]. In this section, an analysis of the fluctuations found in plasma #99896 is given, and their role in producing good thermal confinement is clarified.

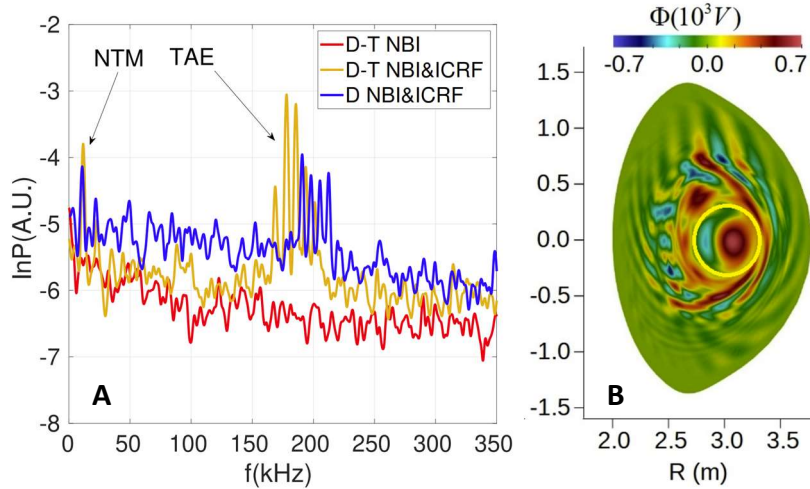


Figure 3: Core plasma fluctuations characteristics. (A) Density fluctuations as obtained from reflectometry at major radius $R \sim 3.36$ m, $\rho \sim 0.35$ and $t = 8.4$ s, for the D-T discharge #99896 with only NBI heating or with full NBI and ICRF heating and comparison to the pure D discharge #100871. (B) Electrostatic potential, Φ , fluctuations obtained for the D-T discharge #99896 by the global code FAR3D when considering two species of energetic ions, H and D, accelerated by the ICRF power. The yellow circle represents the $q = 1$ surface. Inside $q = 1$, a $n = 1$ perturbation is obtained which is identified as a fishbone instability. Outside $q = 1$, TAEs are obtained.

A Fourier analysis of the measured magnetic fluctuations is shown in the supplementary information, Fig. S1(A and B). A full range of activity is found at both low and high frequencies. In the frequency range $1 \text{ kHz} < f < 40 \text{ kHz}$, modes with toroidal mode number $n = 0 - 7$ are detected, while for $120 \text{ kHz} < f < 200 \text{ kHz}$ the modes detected cover $n = -5$ to $n = 6$. However, nonlinear mode-mode interactions are at the origin of some of these fluctuations. This is demonstrated by performing a mode-mode bi-coherence analysis [34]. In particular, the

nonlinear interplay between high-frequency TAE and low-frequency NTM is at the origin of the high frequency perturbations with toroidal mode number $n = 1$ and $n = 2$ among other interactions (this is shown in the supplementary information, Fig.2 S2). A necessary condition for such an interaction to occur is that the radial locations of TAE and NTM are close to each other. This requirement is further verified by the analysis of the location of the different perturbations in real space using several techniques, as clarified in the methods section. RSAE and fishbones are located inside $q = 1$, at $\rho \sim 0.25$, with q the safety factor defined as $q \equiv d\Psi_t/d\Psi_p$ with Ψ_t the toroidal magnetic flux and Ψ_p the poloidal magnetic flux. RSAE are destabilized very close to the magnetic axis. TAE and NTM are located just outside $q = 1$, at $0.25 < \rho < 0.45$.

Further evidence of radial and temporal overlap of MHD and TAE beyond $q = 1$, located at $R \sim 3.25$ m, is obtained from density fluctuations using a reflectometry diagnostic [35] at $R \sim 3.36$ m. It is shown in Fig.3A that high frequency fluctuations for both D-T and D are detected in the TAE and NTM frequency ranges. Furthermore, except for the frequencies corresponding to TAE and NTM, density fluctuations are lower for D-T than for D, notably in the typical range of ITG fluctuations $f < 150$ kHz. This supports the improvement in confinement for the thermal ions shown in Section 2. Density fluctuations do not increase significantly when 4.5 MW of ICRF power is added on top of NBI power, except at the TAE and NTM frequencies. This is important because, in general, turbulence increases with increasing input power leading to the so-called thermal confinement degradation with input power [12].

The origin of the destabilization of magnetic fluctuations by energetic ions has been analyzed with the global gyrofluid code FAR3D [36]. Two energetic ion species, H and D, were considered because they are both ICRF accelerated by means of the first and second harmonic absorption. Their characteristics are obtained from TRANSP. The frequency and location of the fishbone and TAE perturbations obtained from linear simulations with FAR3D agree with experimental data as shown in the supplementary information Fig. S3 and S4, which clarifies that the perturbations are destabilized by ICRF-accelerated ions. Nonlinear simulations including both energetic ion species are shown in Fig.3B. The radial extension of the electrostatic potential perturbation, $2.4 \text{ m} < R < 3.5$ m, agrees well with the experimental location and clearly shows that the energetic-ion-induced perturbations extend up to mid-radius, coinciding with the radial extension of the decreased thermal energy transport losses in D-T compared to D.

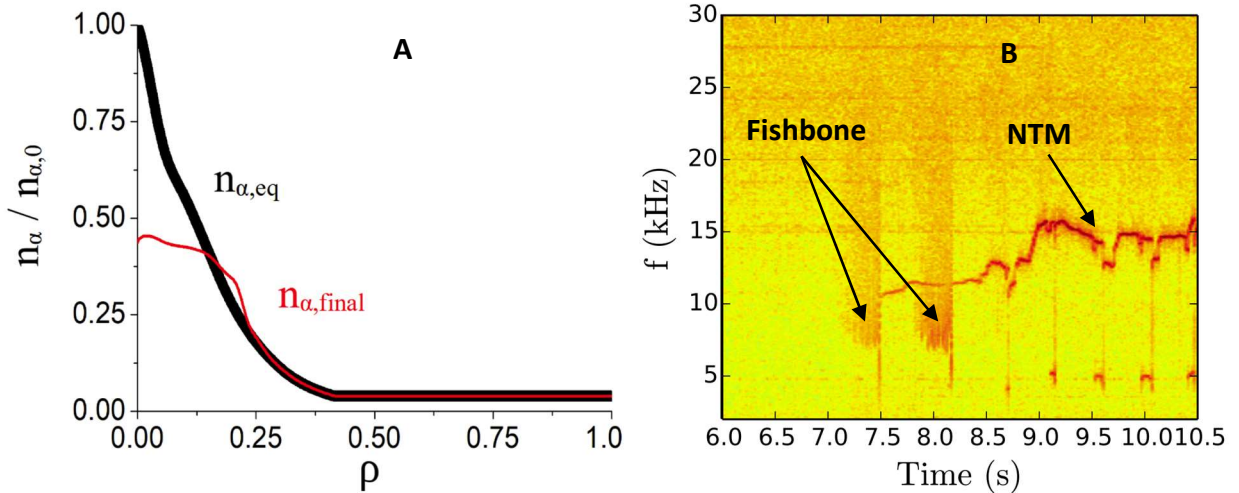


Figure 4: Alpha particle transport and losses in D-T. (A) Alpha particle density profile as calculated with TRANSP assuming no alpha particle transport ($n_{\alpha,eq}$) and comparison to the profile obtained from the FAR3D code after the full development of the fishbone instability ($n_{\alpha,final}$). (B) Alpha particle loss frequency spectrum obtained by using the fast ion loss detector (FILD) with channels that are receptive to 3.5 MeV alpha particles.

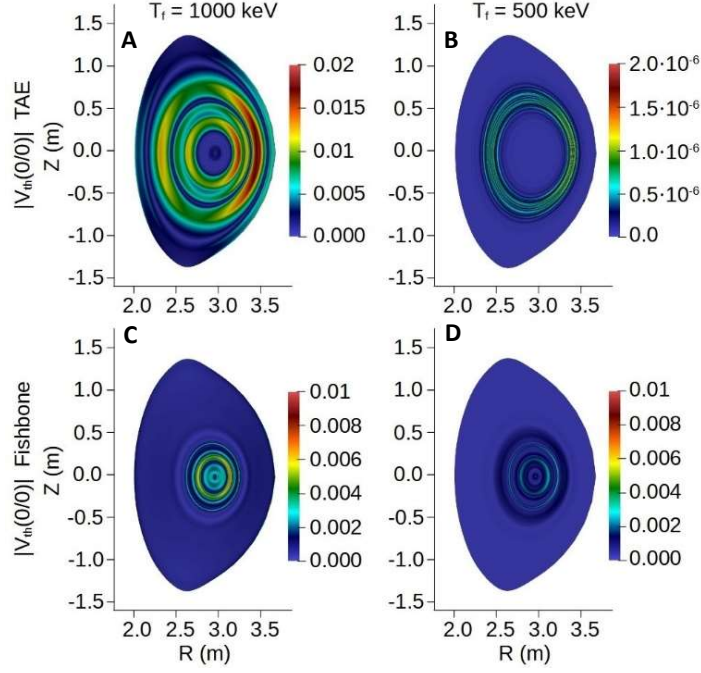


Figure 5: Zonal flow generation by energetic particle instabilities. 2D pattern of $n = 0, m = 0$ structures of zonal poloidal flows, $V_{th}(0,0)$, for the TAE and fishbone instabilities. $V_{th}(0,0)$ is defined as $V_{th}(0,0) = E_r(0,0) \times B\phi$ with $E_r(0,0)$ the $n, m = 0,0$ component of the perturbed radial electric field and $B\phi$ the toroidal magnetic field. The dependence of the zonal flow intensity on the perturbation strength is studied by scanning the energetic ion equivalent temperature (T_f) using two values, $T_f = 1$ MeV and $T_f = 500$ keV in the FAR3D code. Zonal flow generation increases with increasing perturbation intensity for both TAEs (A and B) and fishbones (C and D). The radial extension of zonal flow activity coincides with the extension of the two perturbations.

In addition to the nonlinear interplay between TAE and NTM, other complex and multi-scale interactions are of paramount interest and critically determine the performance. It is found with FAR3D that alpha particles do not destabilize any perturbation due to their low density, however, nonlinear interplay with fishbones can induce radial transport and losses of alpha particles, partially depleting the plasma axis of such particles as shown in Fig.4A. This is experimentally corroborated, as shown in Fig.4B, by means of the fast ion loss detector (FIL) [37]. In the initial phase of the discharge, when the activity of the fishbone is especially strong, alpha particle losses are detected, as can be seen at $t \sim 8$ s. In the later phase of the discharge, fishbone activity is reduced in intensity and no further losses are detected with origin in the fishbone perturbation, but rather in the NTM at $f \sim 15$ kHz. Unlike fishbones, no alpha losses with origin in TAE are detected both in the FAR3D simulations and in the experiment. Therefore, it becomes clear that although magnetic perturbations do not prevent reaching high confinement, they can lead to loss of fusion power. These results show the critical interaction between magnetic perturbations and alpha particles, and we conclude that it is essential to control such interactions in order to produce high fusion power in future tokamak reactors.

Nevertheless, magnetic perturbations induced by energetic ions can also lead to beneficial effects that may have a positive impact on reducing energy losses by heat transport. This is the case of the interplay with the so-called zonal flows, i.e. thermal plasma flows with $f \sim 0$ and poloidal and toroidal perturbation mode numbers, $n, m = 0,0$. Zonal flows were theoretically predicted [38] and also obtained in dedicated numerical simulations in the presence of energetic ions [36][39][40]. They are known to reduce transport driven by ITG turbulence [41], in particular in the presence of energetic MeV ions as shown in D-³He plasmas [32][42].

The generation of zonal flows is studied for discharge #99896 by analyzing the energy transfer between fishbone and TAE perturbations and the thermal plasma. The 2D pattern of $n = 0$ structures for zonal poloidal flows, as obtained from FAR3D nonlinear simulations, are shown in Fig.5(A to D) considering two different energies for the energetic ions. Clearly, fishbones and TAE drive zonal flows, with higher intensity with increased energetic ion energy, and hence stronger instability drive.

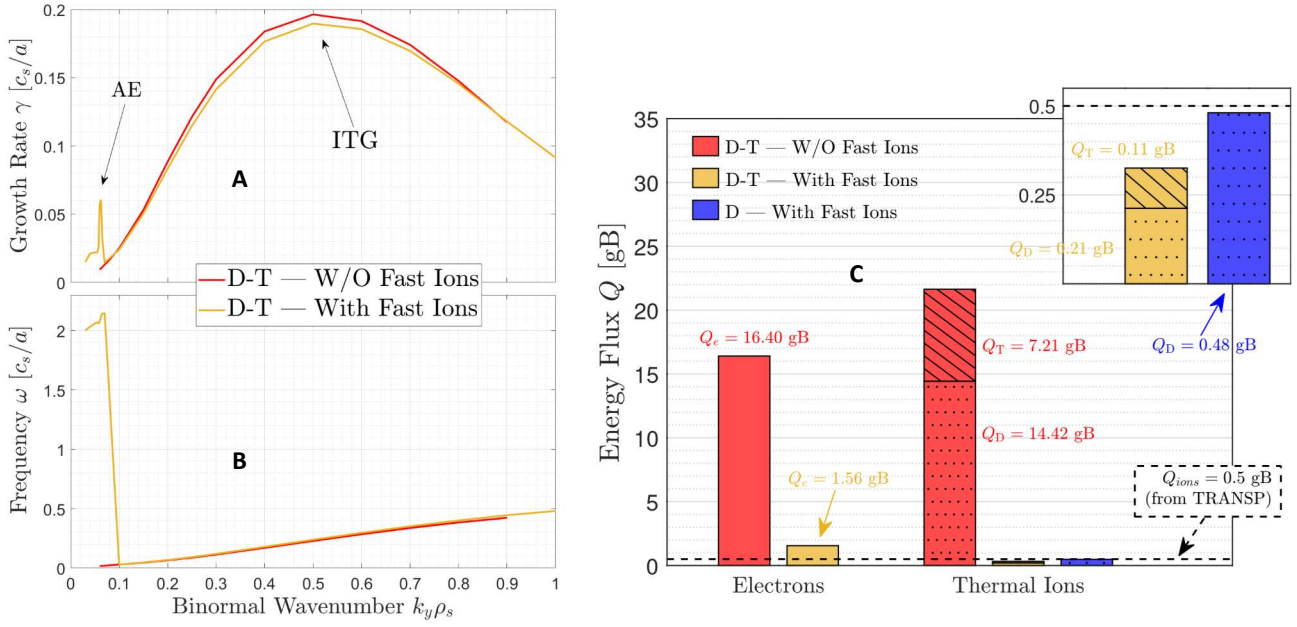


Figure 6: Gyrokinetic analysis of core turbulence reduction in D-T. (A) Growth rate, γ , and (B) frequency, ω , spectrum obtained from linear simulations with the CGYRO code. k_y is the binormal wavenumber normalized to the proton sound gyroradius ρ_s . (C) Energy flux obtained from gyrokinetic simulations performed with the CGYRO code for the discharge #99896 at $\rho = 0.31$. The simulations are performed including and excluding the energetic ion component. Values of the ion thermal energy flux deduced from power balance in TRANSP (black horizontal dashed line) are only obtained when the energetic ion component is included in the simulations as a separate species. The total thermal ion energy flux obtained in D-T including energetic ions is compared to the one obtained assuming that all the thermal ions are D while keeping the rest of the parameters fixed. The energy flux in pure D is significantly higher than in D-T (a zoom of those bars is displayed in the inset on the top right).

The role of T and energetic ions on the good plasma confinement of discharge #99896 is further analyzed by performing simulations with CGYRO [43]. CGYRO solves the gyrokinetic-Maxwell equations [44] to obtain the electrostatic and electromagnetic fluctuations and corresponding turbulent energy transport. Local simulations are performed at $\rho = 0.31$ by including and excluding energetic ions as separate species in addition to the electrons, D and T species. Due to the low energetic ion density compared to the electron density, $\sim 3\%$, the growth rates obtained in linear simulations are nearly unaffected in the ITG scales by the presence of energetic ions as shown in Fig. 6(A and B). However, low k_y modes with TAE frequency are destabilized. These results show that the type of plasma found in JET is different to other plasmas dominated by energetic ions effects, such as the FIRE mode [6], which is characterized by strong turbulence reduction with energetic ion dilution and linear effects [45].

Regarding non-linear effects, as shown in Fig. 6(C), the energy flux, Q , obtained when including energetic ions is more than ten times lower and is close to the values calculated from power balance analysis from TRANSP. Importantly, such a strong reduction in thermal energy flux is accompanied by a high increase in zonal flow shearing activity, $\omega_{E \times B}$, which is five times higher when energetic ions are included and thus confirming the results obtained with FAR3D. Furthermore, there is a clear asymmetry between the transport obtained in D and in T, with the T transport systematically lower than that for D, $\chi_{i,T} \sim 0.8\chi_{i,D}$. Such a difference has an important consequence on the total flux in D-T compared to that of pure D. This is numerically analyzed by performing an alternative simulation in which the T ions are artificially considered as D, thus performing a pure D simulation. The turbulent energy flux ratio $Q_{D-T}/Q_D = 0.67$ is similar to the power balance one obtained for the discharges #100871 in D and #99896 in D-T at the same radial location, $Q_{99896}/Q_{100871} = 0.71$. This result confirms expectations from purely numerical simulations performed for D-T plasmas [46][47][48]. From the numerical point of view, global effects from profile shearing were investigated in CGYRO and found them to negligibly affect the thermal fluxes at the radial location studied.

In summary, the analyses of core plasma fluctuations indicate an optimum route towards the generation of fusion power in D-T tokamak plasmas whereby energetic ion instabilities produced by alpha particles remain in

conditions of negligible or weak alpha particle transport, while they can induce thermal energy transport reduction by means of zonal flows. Importantly, this is obtained in conditions of some energetic ions characteristics relevant to ITER burning plasmas, e.g. the energetic ion density is similar to the one expected in ITER, $\sim 1\%$ [47], avoiding energetic ion dilution as usually happens in strong NBI heated plasmas.

Pedestal formation in D-T

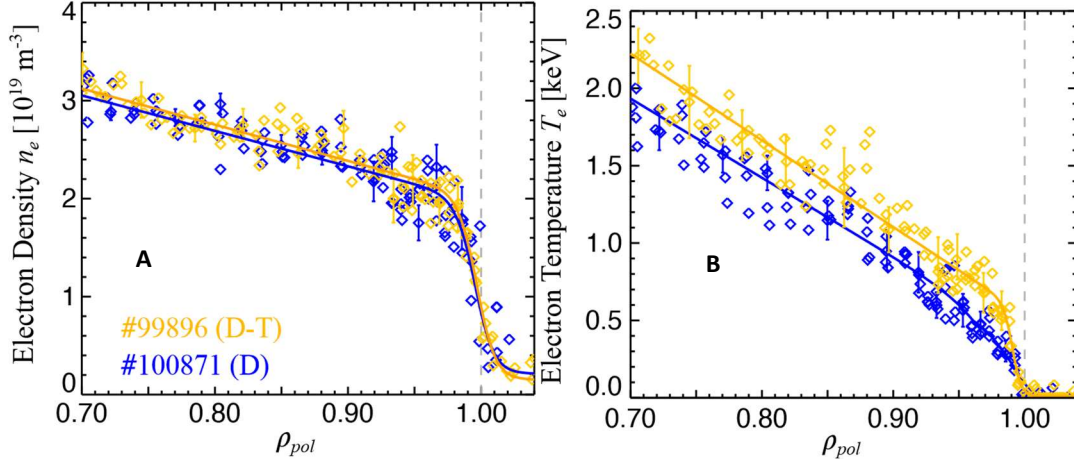


Figure 7: Pedestal formation in D-T and comparison to D.(A) Comparison between edge n_e for the D-T discharge #99896 and D discharge #100871. ρ_{pol} is defined as the normalized poloidal flux. (B) Comparison between edge T_e for the D-T discharge #99896 and D discharge #100871. The vertical dashed line represents the location of the plasma separatrix. The profiles are obtained from HRTS averaged in the time window 8.5 s-8.9 s for #99896 and 8.4 s-8.8 s for #100871.

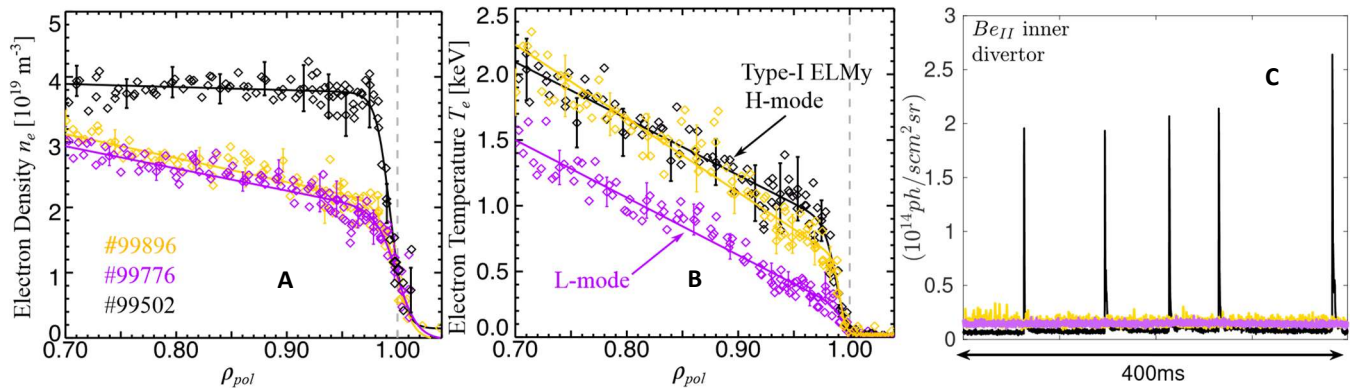


Figure 8: Pedestal characteristics in D-T. Comparison between discharge #99896 and discharge #99502, with $P_{NBI} = 12.5$ MW, in H-mode with type-I ELMs, and #99776, in L-mode, with $P_{NBI} = 5.4$ MW and $P_{ICRF} = 3.3$ MW both obtained at $I_p = 2.5$ MA, $B_T = 3.7$ T and $q_{95} = 4.5$. (A) Edge n_e . (B) Edge T_e . The profiles are obtained from HRTS averaged in the time window 8.5 s-8.9 s for #99896, 7.3 s-7.6 s for #99502 and 8.6 s-8.9 s for #99776. (C) Comparison of the BeII line emission from the inner divertor for the same discharges. The vertical dashed line represents the location of the plasma separatrix.

As depicted in Fig.7 (A and B), the D-T discharge #99896 shows the formation of an H-mode with a steep edge temperature gradient, i.e. a pedestal, at $\rho_{pol} \sim 0.95$. The temperature of the D counterpart is lower at the same location, while the density is nearly identical. The fact that the pedestal pressure is higher with increasing isotope mass has been observed in H-mode plasmas with ELMs (ELMy H-mode). However, in ELMy H-mode regimes with typical type-I ELMs [49][50][51], an increase in edge density rather than temperature is obtained with increasing isotope mass [52].

With the aim of further investigating the origin of the pedestal found in discharge #99896, it is compared to two D-T discharges, one with a clear transition to H-mode with only NBI power and the development of typical type-I ELMy H-mode and another, with NBI and ICRF heating that remains in L-mode, i.e. without temperature pedestal. As shown in Fig.8A, the edge density of the discharges #99896 and the one in L-mode is nearly identical, demonstrating that the density of discharge #99896 remains in L-mode, yet the pedestal formation is evident as the edge temperature nearly reaches that of the ELMy plasma (Fig.8B). Importantly, discharge #99896 has no ELMs as shown in Fig.8C in which the divertor oscillations from BeII divertor emission are compared to those obtained in L-mode and with ELMs. Clearly, the fluctuations are closer to those obtained in L-mode.

The spontaneous generation of plasmas with no ELMs and a pedestal for the temperature is systematic in these kinds of plasmas performed in D-T at different I_p and B_T . It is apparent from the available data that, in those plasma conditions, the input power is close to the L to H-mode transition power threshold, but below the power required to fully develop ELMs. This is supported by the fact that during the phase where the temperature pedestal is sustained an $n = 0$ coherent mode can be observed in the magnetic sensors with a frequency of 5 kHz. This mode, known in JET as M-mode[53], is typically detected in JET immediately after the L to H-mode transition. Long phases with an M-mode present are typically observed in the L-H transition at low density in JET, where pedestal dynamics similar to that described here have been identified [54]. This aspect was further studied in the particular case of discharge #99896, for which it was found that an additional 3 MW of input power lead to the formation of an ELMy H-mode regime. Regarding the magnetic configuration in which these results were obtained, it was used the standard $B \times \nabla B$ in JET with the ion ∇B drift towards the dominant X-point. This configuration is known to be ‘favourable’ in terms of power requirements for the access to H-mode.

These plasmas show similarities with the I-mode regime [55][56][57], found in D, which is characterized by the formation of a pedestal for the temperature, while the density remains in L-mode. Similar to the I-mode, the no-ELM regime described here has good impurity transport properties, with no impurity accumulation. However, no signs of the so-called weakly coherent mode (WCM), typically found in I-mode plasmas, have been detected.

An scenario towards D-T burning plasmas

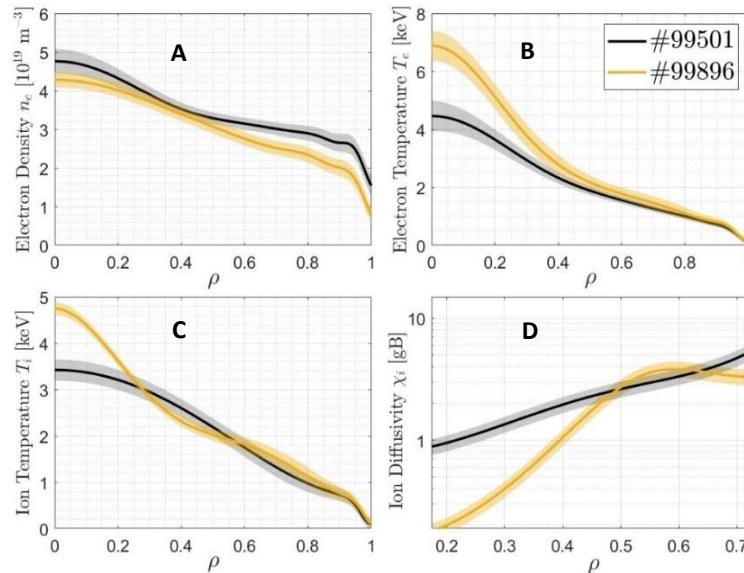


Figure 9: Scenario performance in D-T. Comparison between the discharge #99896, obtained at $P_{NBI}=3.5$ MW, $P_{ICRF}=4.5$ MW, $I_p=1.9$ MA, $B_T=2.8$ T and the D-T discharge #99501, obtained at $P_{NBI}=9.5$ MW, $I_p=2.5$ MA, $B_T=3.7$ T. (A) n_e . (B) T_e . (C) T_i . (D) χ/χ_{GB} . χ_{GB} is the GyroBohm diffusivity defined as $\chi_{GB} = T_e^{3/2} m_p^{1/2} / (e^2 B_T^2 a)$ with m_p the proton mass, e the electron charge and a the plasma minor radius.

Compared to the more typical H modes that develop ELMs and are heated with NBI power, the D-T discharge #99896 provides an attractive alternative with similar thermal energy, but obtained at lower input power, I_p and B_T . Such a feature could lead to a more economical and simpler tokamak design. This is shown in Fig.9(A to C) by comparing the discharge #99896 and the D-T H-mode discharge #99501, at higher P_{NBI} , I_p , and B_T and heated with pure NBI power. Clearly, the density is higher at the edge for the discharge #99501, since a pedestal is formed for both the density and the temperature and yet the total thermal energy content of the two discharges, W_{th} , is similar, $W_{th} \sim 2.4$ MJ. The reason is that the lower edge density is compensated by the higher core temperatures and lower core energy transport losses as shown in Fig.9(D) by comparing χ_i , which is nearly ten times lower in the plasma core for the discharge #99896.

Discussion

The path towards commercial fusion reactors, although better understood in recent decades, still poses physics and technological uncertainties. The size, magnetic configuration, type of confinement or power exhaust techniques expected in future tokamak devices are not fully established. Therefore, it is of fundamental importance to further clarify a safe and clear route toward the generation of efficient energy by means of fusion reactions. This is especially important for D-T plasmas. The presence of T, the generation of a high neutron rate at 14.1 MeV energy, or the presence of alpha particles, are all characteristics of D-T that are not present in ubiquitous pure-D discharges. Studying the impact of such differences is critical in order to properly characterize how D-T fusion reactors might behave. In particular, T can have a strong impact on confinement, impurity generation, and stability, while alpha particles can lead to significant destabilization of magnetic perturbations and provide electron heating.

The JET tokamak has recently performed a new D-T campaign after the first ones were developed at TFTR [8] and JET [9] in the 90's, in order to address some of these points which were not previously studied. A particular emphasis has been put on the exploration of some of the unique features expected in burning D-T plasmas, i.e. simultaneous high electron heating, low rotation, and fully destabilized energetic ions instabilities.

A major result has been obtained suggesting that some reactor-relevant plasma conditions may be very beneficial. A clear reduction of energy losses by turbulence in D-T with respect to D leads to higher confinement plasmas, free of core impurity accumulation, while avoiding dangerous ELMs typical of standard H-modes and thus providing a stable plasma regime. These results confirm how crucial it is to perform experiments in D-T compared to D, as in addition to changes in confinement, burning D-T plasmas can be characterized by a strong nonlinear interplay between different plasma scales in the presence of highly energetic ions. This interplay can induce alpha particle transport and losses but also induce physical mechanisms, such as zonal flows, which can lead to an improved thermal confinement that can compensate for this effect and increase the fusion power generation.

Our findings pave the way for a more economical and simpler design of tokamaks, confirming that nuclear fusion by means of magnetically confined D-T plasmas is a promising source of clean energy. However, further studies, such as compatibility with power exhaust capabilities and exploration at higher density and power, are required to fully qualify these plasmas as a solid route towards tokamak reactors. Furthermore, it is necessary to perform more detailed modeling activities to analyze multiscale effects involving energetic ions and plasma perturbations at different spatial and temporal scales. Specially important is to develop plasmas in which, unlike in the JET results shown in this paper, alpha particle heating is dominant. To this end, the experimental and modeling efforts in D-T including a significant population of alpha particles, as expected in ITER [58] or SPARC[59], are essential.

Methods

Experimental Design

The JET tokamak has investigated some of the most important fusion reactor conditions by conducting a new D-T campaign with Be/W wall. To reproduce the simultaneous high electron heating, low torque, and the destabilization of energetic ions related instabilities expected in future tokamak reactors, JET has mostly used

ICRF power rather than NBI. Several experimental conditions were explored to find an optimum plasma state in terms of confinement, energetic ion production, and D-T fusion power yield. One of the limitations of such exploratory work was the ICRF power, and hence the amount of electron heating available, which was limited to ~ 4.5 MW, whereas the NBI power was used up to 10 MW in pure NBI plasmas. The ICRF frequency used was 55 MHz at $B_T = 3.7$ T and 42 MHz at $B_T = 2.75$ T.

Different scans were performed for I_p and B_T , e.g. I_p was explored in the range $1.9 \text{ MA} < I_p < 2.5 \text{ MA}$ at two $B_T = 2.75$ T, 3.7 T. The D-T concentration ratio was scanned from 40% T to 85% T by using different valves injecting neutral D and T gases.

Key diagnostics for D-T operation

The ion temperature profiles in this paper were obtained from charge exchange recombination spectroscopy (CXRS) [60] measurements of impurity ions and electron temperature profiles from combined analysis of LIDAR Thomson scattering [61] and high-resolution Thomson scattering (HRTS) [62] diagnostics. The density profiles were taken from HRTS measurements, with the density normalized to match the line-average density measured by a far-infrared interferometer.

Mirnov coils are used as a standard MHD diagnostic on almost all tokamak devices. The coils are installed within the vacuum vessel close to the plasma boundary and provide a measurement of the time derivative of the magnetic field. Magnetic spectrograms (Fourier decomposition of the Mirnov coil signal) can then be used to identify relevant oscillation frequencies associated with MHD activity. In JET a number of coil arrays with high-frequency response are available, allowing activity in the Alfvén range to be observed.

The time-resolved neutron yield in JET is measured using three fission chambers, containing ^{235}U and ^{238}U , located outside the vacuum vessel.

The Alfvén eigenmode active diagnostic (AEAD) [63] is characterized by six toroidally spaced antennas, each with independent power and phasing, whose aim is to actively excite marginally stable TAEs.

Alpha particle losses are detected by the fast ion loss detector (FIL) consisting of a Faraday cup array [37]. The Faraday cup array is composed of multiple cups that span a wide poloidal angle below the outboard midplane at a single toroidal location with a minor radial extent.

ELMs are characterized by the BeII emission signal from the inner divertor region.

The plasma isotopic composition is measured at the divertor comparing the relative amplitude of Balmer D_α and T_α spectral lines. The D and T ratio in the plasma core is assumed to be equal to the edge, as is usually the case in JET in the presence of multi-ion plasmas when turbulence is driven by ITG [64].

The JET X-mode reflectometry diagnostic [35] is composed of four distinct radial correlation reflectometers. All these reflectometers probe the mid-plane JET plasma. Plasma fluctuations can be obtained from the phase fluctuations of the reflectometer signal.

Magnetic perturbation spatial location and q profile verification

The q profile for discharge #99896 has been obtained by means of a loop between the EFIT code and the TRANSP code. The EFIT code calculates the magnetic equilibrium with the input data for the energetic ions content from TRANSP simulations. After a few iterations, a converged q profile is obtained. The validation of the q profile obtained from TRANSP and used for modeling with FAR3D was carried out against a series of diagnostics and MHD markers. As markers with the strongest signature in the diagnostics, the destabilised NTMs were identified and their toroidal mode number calculated using a toroidal array of Mirnov coils. The radial location of the associated rational surface $q=4/3$ was inferred using two methods: the first uses as proxy the location of the phase inversion of the perturbed electron temperature derived from Electron Cyclotron Emission (ECE) at the NTM frequency, the second matched the NTM frequency as derived from the Mirnov coils to the Doppler-shifted plasma rotation i.e. $n \times V_{phi}$, where V_{phi} is the toroidal rotation of the main plasma ions as derived from CXRS diagnostic. The radial location of the $q=1/1$ surface was inferred from the inversion radius of the ECE temperature profile during sawtooth crashes as well as from the fishbones signatures in the perturbed plasma temperature from ECE, evidencing a typical kink-like pattern inside the $q=1$ surface. Lastly, the RSAEs and TAEs were located using Soft X-ray cameras, interferometry and reflectometry.

Experimental profiles fitting

The profile fitting algorithm makes use of a Gaussian process regression (GPR), which is not limited by a selection of specific fit functions and provides a statistically rigorous estimation of the confidence bounds of the fit. For more details, see the book on the topic written by Carl Edward Rasmussen and Christopher K. I. Williams <http://gaussianprocess.org/gpml/chapters/>

TRANSP simulations

The pulses shown in this article were analyzed by interpretive simulations performed with the TRANSP modelling suite [65] coupled with external heating modules NUBEAM (NBI) [66] and TORIC (ICRF) [67], and prepared with the OMFIT integrated modelling platform [68]. Interpretive analysis was based on the use of fitted profiles, including electron density and temperatures. The fitting of T_e , n_e and T_i were performed on data obtained from HRTS and CXRS. The fitting of experimental profiles consists on applying a global third-order polynomial fit in the range $\rho \lesssim 0.8$ (with the additional constraint $\partial T_i(0)/\partial r = 0$).

FAR3D description and simulations parameters

The gyrofluid FAR3D code solves the linear and nonlinear reduced resistive MHD equations describing the thermal plasma evolution coupled with the first two moments of the gyro-kinetic equation, the equations of the energetic particle density and parallel velocity moments [69] [70], introducing the wave-particle resonance effects required for Landau damping/growth. The correct model calibration requires performing gyrokinetic simulations to calculate the Landau closure coefficients in the gyrofluid simulations, matching the analytic TAE growth rates of the two-pole approximation of the plasma dispersion function with a Lorentzian energy distribution function for the energetic particles. The lowest order Lorentzian is matched with a Maxwellian distribution by choosing an equivalent average energy. Further details of the model equations can be found in references [71][72].

A set of linear simulations are performed to reproduce the Alfvén eigenmode (AE) activity observed in the discharge, identifying the resonance induced by populations of energetic particles (EP) as passing D and trapped H. The analysis is based on a parametric study with respect to the EP beta (EP density in the plasma) and energy, calculating AEs consistent with the frequency range, plasma radial location, modes number and AE family observed in the experiment. Nonlinear simulations including passing D and trapped H populations are performed to analyze the saturation phase of the AE instabilities, particularly the energetic particle transport induced, the generation of zonal structure, and the nonlinear interaction between different EP populations. The simulations are performed using the EP model profiles obtained from TRANSP, the measured thermal plasma profiles, and the equilibrium calculated with VMEC code [73].

CGYRO description and simulations parameters

Table 1: Employed plasma parameters in CGYRO simulations modelling JET pulse #99896 at $\rho = 0.31$ and $t = 8.6$ s.

ϵ	q	\hat{s}	T_i/T_e	a/L_{n_e}	a/L_{T_e}	a/L_{T_i}	n_D/n_e	n_T/n_e	a/L_{n_D}
0.30	1.17	0.74	0.76	1.00	3.20	2.40	0.58	0.39	0.93
a/L_{n_T}	n/n_e	T_f/T_e	β_e (%)	v_{ee}/c_s	B_0 (T)	T_e (keV)	n_e (m^{-3})	a (m)	R_0 (m)
0.92	0.03	21.0	0.44	0.39	2.75	3.68	$3.67 \cdot 10^{19}$	0.91	3.00

Here, ϵ represents the inverse aspect ratio, q the safety factor, \hat{s} the magnetic shear, n the species density normalized to the electron density, $a/L_{n,T}$ the normalized logarithmic density and temperature gradient, β_e the electron-beta, v_{ee} the electron collision rate and a the minor radius. The normalization factors in standard units are also reported, i.e. the on-axis magnetic field strength B_0 , the local ($\rho = 0.31$) electron temperature T_e , density n_e and the major radius R_0 .

The CGYRO code [43] solves the electromagnetic gyrokinetic-Maxwell equations [44]. Local simulations were carried out at $\rho = 0.31$. Shaped, up-down symmetric flux-surface geometry was used and multi-species collisions were included using the Sugama collision operator [74]. Transverse and compressional electromagnetic fluctuations were retained. Rotation effects were assumed to be small in the core and not included. Kinetic electrons, D and T as separate species, were included in the simulations. Regarding the energetic-ion species, a lumped H-D species with effective mass averaged between H and D was assumed and modeled by fitting the energetic particle distribution to an equivalent high temperature Maxwellian equilibrium distribution.

The simulations used a radial box length of $L_x = 673\rho_s$ and a binormal box of length $L_y = 628\rho_s$. $N_r = 768$ radial modes and $N_\alpha = 64$ complex toroidal modes were retained. Other resolution parameters were: $N_\theta = 24$ (field line resolution), $N_\xi = 24$ (pitch-angle resolution), $N_u = 8$ (energy resolution) with maximum energy $u^2_{max} = 8$. The definitions of the CGYRO numerical resolution parameters can be found in [43]. The energy flux is provided in GB unit defined as $Q_{GB} = n_e T_e c_s \rho_*^2$, with $c_s = \sqrt{T_e/m_p}$, $\rho_* = \rho_s/a$ is the ratio of the proton sound gyroradius, $\rho_s = c_s/\Omega_c$, to the system size, with $\Omega_c = eB_0/m_p$ the ion gyrofrequency. Convergence test have been performed indicating that the CGYRO results are well resolved.

The zonal flow shearing is defined in CGYRO as:

$$\omega_{E \times B} = \sum_{k_x} k_x^2 \rho_s^2 \langle |\hat{\Phi}(k_y, k_x)|^2 \rangle_t |_{k_y=0}$$

where k_x is the radial wavenumber, $\hat{\Phi}(k_y, k_x)$ is the fluctuating electrostatic potential and $\langle \rangle_t$ denotes the temporal average

The equilibrium profile and geometry parameters are given in Table 1.

Data availability

The JET experimental data is stored in the PPF (Processed Pulse File) system which is a centralised data storage and retrieval system for data derived from raw measurements within the JET Torus, and from other sources such as simulation programs. These data are fully available for the EUROfusion consortium members and can be accessed by non-members under request to EUROfusion.

Numerical data that support the outcome of this study are available from the corresponding author upon request.

Code availability

The research codes cited in the paper require a prior detailed knowledge of the implemented physics models and are under continuous development. The corresponding author can be contacted for any further information.

References

- [1] V.P. Smirnov. Tokamak foundation in ussr/russia 1950–1990. *Nuclear Fusion*, 50(1):014003, dec 2009. doi: 10.1088/0029-5515/50/1/014003. URL <https://dx.doi.org/10.1088/0029-5515/50/1/014003>.
- [2] J. Ongena, R. Koch, R. Wolf, and H. Zohm. Magnetic-confinement fusion. *Nature Physics*, 12(5):398–410, 2016.
- [3] F. Wagner, G. Fussmann, T. Grave, M. Keilhacker, M. Kornherr, K. Lackner, K. McCormick, E. R. Muller, A. Stabler, G. Becker, K. Bernhardt, U. Ditte, A. Eberhagen, O. Gehre, J. Gernhardt, G. v. Gierke, E. Glock, O. Gruber, G. Haas, M. Hesse, G. Janeschitz, F. Karger, S. Kissel, O. Klu"ber, G. Lisitano, H. M. Mayer, D. Meisel, V. Mertens, H. Murmann, W. Poschenrieder, H. Rapp, H. R"ohr, F. Ryter, F. Schneider, G. Siller, P. Smeulders, F. Soldner, E. Speth, K. H. Steuer, Z. Szymanski, and O. Vollmer. Development of an edge transport barrier at the h-mode transition of asdex. *Phys. Rev. Lett.*, 53:1453–1456, Oct 1984. doi: 10.1103/PhysRevLett.53.1453. URL <https://link.aps.org/doi/10.1103/PhysRevLett.53.1453>.

- [4] J. W. Connor, T. Fukuda, X. Garbet, C. Gormezano, V. Mukhovatov, M. Wakatani, the ITB Database Group, and the ITPA Topical Group on Transport and Internal Barrier Physics. *Nucl. Fusion*, 44:R1–R49, 2004.
- [5] Yuntao Song, Xiaolan Zou, Xianzu Gong, Alain Becoulet, Richard Buttery, Paul Bonoli, Tuong Hoang, Rajesh Maingi, Jinping Qian, Xiaoming Zhong, Adi Liu, Erzhong Li, Rui Ding, Juan Huang, Qing Zang, Haiqing Liu, Liang Wang, Ling Zhang, Guoqiang Li, Youwen Sun, Andrea Garofalo, Tom Osborne, Tony Leonard, Seung Gyou Baek, Greg Wallace, Liqing Xu, Bin Zhang, Shouxin Wang, Yuqi Chu, Tao Zhang, Yanmin Duan, Hui Lian, Xuexi Zhang, Yifei Jin, Long Zeng, Bo Lyu, Binjia Xiao, Yao Huang, Yong Wang, Biao Shen, Nong Xiang, Yu Wu, Jiefeng Wu, Xiaojie Wang, Bojiang Ding, Miaohui Li, Xinjun Zhang, Chengming Qin, Weibin Xi, Jian Zhang, Liansheng Huang, Damao Yao, Yanlan Hu, Guizhong Zuo, Qiping Yuan, Zhiwei Zhou, Mao Wang, Handong Xu, Yahong Xie, Zhengchu Wang, Junling Chen, Guosheng Xu, Jiansheng Hu, Kun Lu, Fukun Liu, Xinchao Wu, Baonian Wan, Jiengang Li, and EAST Team. Realization of thousand-second improved confinement plasma with super i-mode in tokamak east. *Science Advances*, 9(1):eabq5273, 2023. doi: 10.1126/sciadv.abq5273. URL <https://www.science.org/doi/abs/10.1126/sciadv.abq5273>.
- [6] H. Han, S. J. Park, C. Sung, J. Kang, Y. H. Lee, J. Chung, T. S. Hahm, B. Kim, J.-K. Park, J. G. Bak, M. S. Cha, G. J. Choi, M. J. Choi, J. Gwak, S. H. Hahn, J. Jang, K. C. Lee, J. H. Kim, S. K. Kim, W. C. Kim, J. Ko, W. H. Ko, C. Y. Lee, J. H. Lee, J. K. Lee, J. P. Lee, K. D. Lee, Y. S. Park, J. Seo, S. M. Yang, S. W. Yoon, and Y.-S. Na. A sustained high-temperature fusion plasma regime facilitated by fast ions. *Nature*, 609(7926):269–275, Sep 2022. ISSN 1476-4687. doi: 10.1038/s41586-022-05008-1. URL <https://doi.org/10.1038/s41586-022-05008-1>.
- [7] H Zohm. Edge localized modes (ELMs). *Plasma Physics and Controlled Fusion*, 38(2):105–128, feb 1996. doi: 10.1088/0741-3335/38/2/001. URL <https://doi.org/10.1088/0741-3335/38/2/001>.
- [8] J D Strachan, S Batha, M Beer, M G Bell, R E Bell, A Belov, H Berk, S Bernabei, M Bitter, B Breizman, N L Bretz, R Budny, C E Bush, J Callen, S Cauffman, C S Chang, Z Chang, C Z Cheng, D S Darrow, R O Dendy, W Dorland, H Duong, P C Efthimion, D Ernst, H Evenson, N J Fisch, R Fisher, R J Fonck, E D Fredrickson, G Y Fu, H P Furth, N N Gorelenkov, V Ya Goloborod'ko, B Grek, L R Grisham, G W Hammett, R J Hawryluk, W Heidbrink, H W Herrmann, M C Herrmann, K W Hill, J Hogan, B Hooper, J C Hosea, W A Houlberg, M Hughes, D L Jassby, F C Jobes, D W Johnson, R Kaita, S Kaye, J Kesner, J S Kim, M Kissick, A V Krasilnikov, H Kugel, A Kumar, N T Lam, P Lamarche, B Leblanc, F M Levinton, C Ludescher, J Machuzak, R P Majeski, J Manickam, D K Mansfield, M Mauel, E Mazzucato, J McChesney, D C McCune, G McKee, K M McGuire, D M Meade, S S Medley, D R Mikkelsen, S V Mirnov, D Mueller, Y Nagayama, G A Navratil, R Nazikian, M Okabayashi, M Osakabe, D K Owens, H K Park, W Park, S F Paul, M P Petrov, C K Phillips, M Phillips, P Phillips, A T Ramsey, B Rice, M H Redi, G Rewoldt, S Reznik, A L Roquemore, J Rogers, E Ruskov, S A Sabbagh, M Sasao, G Schilling, G L Schmidt, S D Scott, I Semenov, T Senko, C H Skinner, T Stevenson, E J Strait, B C Stratton, W Stodiek, E Synakowski, H Takahashi, W Tang, G Taylor, M E Thompson, S von Goeler, A von Halle, R T Walters, S Wang, R White, R M Wieland, M Williams, J R Wilson, K L Wong, G A Wurden, M Yamada, V Yavorski, K M Young, L Zakharov, M C Zarnstorff, and S J Zweben. Tfr dt experiments. *Plasma Physics and Controlled Fusion*, 39(12B):B103, dec 1997. doi: 10.1088/0741-3335/39/12B/008. URL <https://dx.doi.org/10.1088/0741-3335/39/12B/008>.
- [9] J. Jacquiot, V.P. Bhatnagar, J.G. Cordey, L.D. Horton, D.F.H. Start, R. Barnsley, P. Breger, J.P. Christiansen, S. Clement, S.J. Davies, J.K. Ehrenberg, L.-G. Eriksson, G.M. Fishpool, M. Gadeberg, P.J. Harbour, H.J. Jäckel, K. Lawson, J. Lingertat, C.G. Lowry, C.F. Maggi, G.F. Matthews, R.D. Monk, D.P. O'Brien, E. Righi, G. Saibene, R. Sartori, B. Schunke, A.C.C. Sips, M.F. Stamp, D. Stork, J.D. Strachan, A. Tanga, K. Thomsen, and JET Team. Overview of iter physics deuterium-tritium experiments in jet. *Nuclear Fusion*, 39(2):235, feb 1999. doi: 10.1088/0029-5515/39/2/307. URL <https://dx.doi.org/10.1088/0029-5515/39/2/307>.
- [10] M.N.A. Beurskens, C. Angioni, S. A. Bozhenkov, O. Ford, C. Kiefer, P. Xanthopoulos, Y. Turkin, J.A. Alcusón, J.P. Baehner, C. Beidler, G. Birkenmeier, E. Fable, G. Fuchert, B. Geiger, O. Grulke, M. Hirsch, M. Jakubowski, H.P. Laqua, A. Langenberg, S. Lazerson, N. Pablant, M. Reisner, P. Schneider, E.R. Scott, T. Stange, A. von Stechow, J. Stober, U. Stroth, Th. Wegner, G. Weir, D. Zhang, A. Zocco, R.C. Wolf, H. Zohm, the W7-X Team, the ASDEX Upgrade Team, and the EUROfusion MST1 Team. Confinement in electron heated plasmas in wendelstein 7-x and asdex upgrade; the necessity to control turbulent transport. *Nuclear Fusion*, 62(1):016015, dec 2021. doi: 10.1088/1741-4326/ac36f1. URL <https://dx.doi.org/10.1088/1741-4326/ac36f1>.

- [11] T. S. Hahm and K. H. Burrell. Flow shear induced fluctuation suppression in finite aspect ratio shaped tokamak plasma. *Physics of Plasmas*, 2(5):1648–1651, 05 1995. ISSN 1070-664X. doi: 10.1063/1.871313. URL <https://doi.org/10.1063/1.871313>.
- [12] E. J. Doyle et al. Chapter 2: Plasma confinement and transport. *Nuclear Fusion*, 47(6):S18, 2007.
- [13] A. Fasoli et al. Chapter 5: Physics of energetic ions. *Nuclear Fusion*, 47:S264, 2007.
- [14] N. Gorelenkov, S. D. Pinches, and K Toi. Energetic particle physics in fusion research in preparation for burning plasma experiments. *Nuclear Fusion*, 54(12):125001, 2014.
- [15] Y Todo. Introduction to the interaction between energetic particles and Alfvén eigenmodes in toroidal plasmas. *Reviews of Modern Plasma Physics*, 3(1):1, 2019.
- [16] W. W. Heidbrink and R. B. White. Mechanisms of energetic-particle transport in magnetically confined plasmas. *Physics of Plasmas*, 27(3):030901, 2020.
- [17] J. Mailloux, N. Abid, K. Abraham, P. Abreu, O. Adabonyan, P. Adrich, V. Afanasev, M. Afzal, T. Ahlgren, L. Aho-Mantila, N. Aiba, M. Airila, M. Akhtar, R. Albanese, M. Alderson-Martin, D. Alegre, S. Aleiferis, A. Aleksa, A.G. Alekseev, E. Alessi, P. Aleynikov, J. Alguacil, M. Ali, M. Allinson, B. Alper, E. Alves, G. Ambrosino, R. Ambrosino, V. Amosov, E. Andersson Sundén, P. Andrew, B.M. Angelini, C. Angioni, I. Antoniou, L.C. Appel, C. Appelbee, S. Aria, M. Ariola, G. Artaserse, W. Arter, V. Artigues, N. Asakura, A. Ash, N. Ashikawa, V. Aslanyan, M. Astrain, O. Asztalos, D. Auld, F. Auriemma, Y. Austin, L. Avotina, E. Aymerich, A. Baciero, F. Bairaktaris, J. Balbin, L. Balbinot, I. Balboa, M. Balden, C. Balshaw, N. Balshaw, V.K. Bandaru, J. Banks, Yu.F. Baranov, C. Barcellona, A. Barnard, M. Barnard, R. Barnsley, A. Barth, M. Baruzzo, S. Barwell, M. Bassan, A. Batista, P. Batistoni, L. Baumane, B. Bauvir, L. Baylor, P.S. Beaumont, D. Beckett, A. Begolli, M. Beidler, N. Bekris, M. Beldishevski, E. Belli, F. Belli, E. Belonohy, M. Ben Yaala, J. Benayas, J. Bentley, H. Bergsaker, J. Bernardo, M. Bernert, M. Berry, L. Bertalot, H. Betar, M. Beurskens, S. Bickerton, B. Bieg, J. Bielecki, A. Bierwage, T. Biewer, R. Bilato, P. Bilková, G. Birkenmeier, H. Bishop, J.P.S. Bizarro, J. Blackburn, P. Blanchard, P. Blatchford, V. Bobkov, A. Boboc, P. Bohm, T. Bohm, I. Bolshakova, T. Bolzonella, N. Bonanomi, D. Bonfiglio, X. Bonnin, P. Bonofiglio, S. Boock, A. Booth, J. Booth, D. Borba, D. Borodin, I. Borodkina, C. Boulbe, C. Bourdelle, M. Bowden, K. Boyd, I. Božičević Mihalić, S.C. Bradnam, V. Braic, L. Brandt, R. Bravanec, B. Breizman, A. Brett, S. Brezinsek, M. Brix, K. Bromley, B. Brown, D. Brunetti, R. Buckingham, M. Buckley, R. Budny, J. Buermans, H. Bufferand, P. Buratti, A. Burgess, A. Buscarino, A. Busse, D. Butcher, E. de la Cal, G. Calabrò, L. Calacci, R. Calado, Y. Camenen, G. Canal, B. Cannas, M. Cappelli, S. Carcangiu, P. Card, A. Cardinali, P. Carman, D. Carnevale, M. Carr, D. Carralero, L. Carraro, I.S. Carvalho, P. Carvalho, I. Casiraghi, F.J. Casson, C. Castaldo, J.P. Catalan, N. Catarino, F. Causa, M. Cavedon, M. Cecconello, C.D. Challis, B. Chamberlain, C.S. Chang, A. Chankin, B. Chapman, M. Chernyshova, A. Chiariello, P. Chmielewski, A. Chomiczewska, L. Chone, G. Ciraolo, D. Ciric, J. Citrin, L. Ciupinski, M. Clark, R. Clarkson, C. Clements, M. Cleverly, J.P. Coad, P. Coates, A. Cobalt, V. Coccoresse, R. Coelho, J.W. Coenen, I.H. Coffey, A. Colangeli, L. Colas, C. Collins, J. Collins, S. Collins, D. Conka, S. Conroy, B. Conway, N.J. Conway, D. Coombs, P. Cooper, S. Cooper, C. Corradino, G. Corrigan, D. Coster, P. Cox, T. Craciunescu, S. Cramp, C. Crapper, D. Craven, R. Craven, M. Crialesi Esposito, G. Croci, D. Croft, A. Croitoru, K. Cromb'e, T. Cronin, N. Cruz, C. Crystal, G. Cseh, A. Cufar, A. Cullen, M. Curuia, T. Czarski, H. Dabirikhah, A. Dal Molin, E. Dale, P. Dalglish, S. Dalley, J. Dankowski, P. David, A. Davies, S. Davies, G. Davis, K. Dawson, S. Dawson, I.E. Day, M. De Bock, G. De Temmerman, G. De Tommasi, K. Deakin, J. Deane, R. Dejarnac, D. Del Sarto, E. Delabie, D. Del-Castillo-Negrete, A. Dempsey, R.O. Dendy, P. Devynck, A. Di Siena, C. Di Troia, T. Dickson, P. Dinca, T. Dittmar, J. Dobrashian, R.P. Doerner, A.J.H. Donn'e, S. Dorling, S. Dormido-Canto, D. Douai, S. Dowson, R. Doyle, M. Dreval, P. Drewelow, P. Drews, G. Drummond, Ph. Duckworth, H. Dudding, R. Dumont, P. Dumortier, D. Dunai, T. Dunatov, M. Dunne, I. Duran, F. Durodi'e, R. Dux, A. Dvornova, R. Eastham, J. Edwards, Th. Eich, A. Eichorn, N. Eidietis, A. Eksaeva, H. El Haroun, G. Ellwood, C. Elsmore, O. Embreus, S. Emery, G. Ericsson, B. Eriksson, F. Eriksson, J. Eriksson, L.G. Eriksson, S. Ertmer, S. Esquembri, A.L. Esquisabel, T. Estrada, G. Evans, S. Evans, E. Fable, D. Fagan, M. Faitsch, M. Falessi, A. Fanni, A. Farahani, I. Farquhar, A. Fasoli, B. Faugeras, S. Fazinić, F. Felici, R. Felton, A. Fernandes, H.

Fernandes, J. Ferrand, D.R. Ferreira, J. Ferreira, G. Ferr`o, J. Fessey, O. Ficker, A.R. Field, A. Figueiredo, J. Figueiredo, A. Fil, N. Fil, P. Finburg, D. Fiorucci, U. Fischer, G. Fishpool, L. Fittill, M. Fitzgerald, D. Flammini, J. Flanagan, K. Flinders, S. Foley, N. Fonnesu, M. Fontana, J.M. Fontdecaba, S. Forbes, A. Formisano, T. Fornal, L. Fortuna, E. Fortuna-Zalesna, M. Fortune, C. Fowler, E. Fransson, L. Frassinetti, M. Freisinger, R. Fresa, R. Fridstr`om, D. Frigione, T. Fu`llop, M. Furseman, V. Fusco, S. Futatani, D. Gadariya, K. Gal, D. Galassi, K. Galazka, S. Galeani, D. Gallart, R. Galv`ao, Y. Gao, J. Garcia, M. Garc´ia-Mun`oz, M. Gardener, L. Garzotti, J. Gaspar, R. Gatto, P. Gaudio, D. Gear, T. Gebhart, S. Gee, M. Gelfusa, R. George, S.N. Gerasimov, G. Gervasini, M. Gethins, Z. Ghani, M. Gherendi, F. Ghezzi, J.C. Giacalone, L. Giacomelli, G. Giacometti, C. Gibson, K.J. Gibson, L. Gil, A. Gillgren, D. Gin, E. Giovannozzi, C. Giroud, R. Glen, S. Gl`ogglar, J. Goff, P. Gohil, V. Goloborodko, R. Gomes, B. Gonc`alves, M. Goniche, A. Goodyear, S. Gore, G. Gorini, T. G`orler, N. Gotts, R. Goulding, E. Gow, B. Graham, J.P. Graves, H. Greuner, B. Grierson, J. Griffiths, S. Griph, D. Grist, W. Gromelski, M. Groth, R. Grove, M. Gruca, D. Guard, N. Gupta, C. Gurl, A. Gusarov, L. Hackett, S. Hacquin, R. Hager, L. H`agg, A. Hakola, M. Halitovs, S. Hall, S.A. Hall, S. Hallworth-Cook, C.J. Ham, D. Hamaguchi, M. Hamed, C. Hamlyn-Harris, K. Hammond, E. Harford, J.R. Harrison, D. Harting, Y. Hatano, D.R. Hatch, T. Haupt, J. Hawes, N.C. Hawkes, J. Hawkins, T. Hayashi, S. Hazael, S. Hazel, P. Heesterman, B. Heidbrink, W. Helou, O. Hemming, S.S. Henderson, R.B. Henriques, D. Hepple, J. Herfindal, G. Hermon, J. Hill, J.C. Hillesheim, K. Hizanidis, A. Hjalmarsson, A. Ho, J. Hobirk, O. Hoenen, C. Hogben, A. Hollingsworth, S. Hollis, E. Hollmann, M. Holzl, B. Homan, M. Hook, D. Hopley, J. Hor`a`cek, D. Horsley, N. Horsten, A. Horton, L.D. Horton, L. Horvath, S. Hotchin, R. Howell, Z. Hu, A. Huber, V. Huber, T. Huddleston, G.T.A. Huijsmans, P. Huynh, A. Hynes, M. Iliasova, D. Imrie, M. Imr`ı`sek, J. Ingleby, P. Innocente, K. Insulander Bj`ork, N. Isernia, I. Ivanova-Stanik, E. Ivings, S. Jablonski, S. Jachmich, T. Jackson, P. Jacquet, H. J`arleblad, F. Jaulmes, J.Jenaro Rodriguez, I. Jepu, E. Joffrin, R. Johnson, T. Johnson, J. Johnston, C. Jones, G. Jones, L. Jones, N. Jones, T. Jones, A. Joyce, R. Juarez, M. Juvonen, P. Kalnin_a, T. Kaltiaisena, J. Kaniewski, A. Kantor, A. Kappatou, J. Karhunen, D. Karkinsky, Yu Kashchuk, M. Kaufman, G. Kaveney, Ye.O. Kazakov, V. Kazantzidis, D.L. Keeling, R. Kelly, M. Kempenaars, C. Kennedy, D. Kennedy, J. Kent, K. Khan, E. Khilkevich, C. Kiefer, J. Kilpelainen, C. Kim, Hyun-Tae Kim, S.H. Kim, D.B. King, R. King, D. Kinna, V.G. Kiptily, A. Kirjasuo, K.K. Kirov, A. Kirschner, T. Kiviniemi, G. Kizane, M. Klas, C. Klepper, A. Klix, G. Kneale, M. Knight, P. Knight, R. Knights, S. Knipe, M. Knolker, S. Knott, M. Kocan, F. K`ochl, I. Kodeli, Y. Kolesnichenko, Y. Kominis, M. Kong, V. Korovin, B. Kos, D. Kos, H.R. Koslowski, M. Kotschenreuther, M. Koubiti, E. Kowalska-Strzeciwillk, K. Koziol, A. Krasilnikov, V. Krasilnikov, M. Kresina, K. Krieger, N. Krishnan, A. Krivska, U. Kruezi, I. Ksiaz`ek, A.B. Kukushkin, H. Kumpulainen, T. Kurki-Suonio, H. Kurotaki, S. Kwak, O.J. Kwon, L. Laguardia, E. Lagzdina, A. Lahtinen, A. Laing, N. Lam, H.T. Lambertz, B. Lane, C. Lane, E.Lascas Neto, E. L aszyn`ska, K.D. Lawson, A. Lazaros, E. Lazzaro, G. Learoyd, Chanyoung Lee, S.E. Lee, S. Leerink, T. Leeson, X. Lefebvre, H.J. Leggate, J. Lehmann, M. Lehnen, D. Leichtle, F. Leipold, I. Lengar, M. Lennholm, E. Leon Gutierrez, B. Lepiavko, J. Lepp`anen, E. Lerche, A. Lescinskis, J. Lewis, W. Leysen, L. Li, Y. Li, J. Likonen, Ch. Linsmeier, B. Lipschultz, X. Litaudon, E. Litherland-Smith, F. Liu, T. Loarer, A. Loarte, R. Lobel, B. Lomanowski, P.J. Lomas, J.M. L`opez, R. Lorenzini, S. Loreti, U. Losada, V.P. Loschiavo, M. Loughlin, Z. Louka, J. Lovell, T. Lowe, C. Lowry, S. Lubbad, T. Luce, R. Lucock, A. Lukin, C. Luna, E.de la Luna, M. Lungaroni, C.P. Lungu, T. Lunt, V. Lutsenko, B. Lyons, A. Lysoivan, M. Machielsen, E. Macusova, R. M`aenp`a`a, C.F. Maggi, R. Maggiora, M. Magness, S. Mahesan, H. Maier, R. Maingi, K. Malinowski, P. Manas, P. Mantica, M.J. Mantsinen, J. Manyer, A. Manzanares, Ph. Maquet, G. Marceca, N. Marcenko, C. Marchetto, O. Marchuk, A. Mariani, G. Mariano, M. Marin, M. Marinelli, T. Markovi`c, D. Marocco, L. Marot, S. Marsden, J. Marsh, R. Marshall, L. Martellucci, A. Martin, A.J. Martin, R. Martone, S. Maruyama, M. Maslov, S. Masuzaki, S. Matejck, M. Mattei, G.F. Matthews, D. Matveev, E. Matveeva, A. Mauriya, F. Maviglia, M. Mayer, M.-L. Mayoral, S. Mazzi, C. Mazzotta, R. McAdams, P.J. McCarthy, K.G. McClements, J. McClenaghan, P. McCullen, D.C. McDonald, D. McGuckin, D. McHugh, G. McIntyre, R. McKean, J. McKehon, B. McMillan, L. McNamee, A. McShee, A. Meakins, S. Medley, C.J. Meekes, K. Meghani, A.G. Meigs, G. Meisl, S. Meitner, S. Menmuir, K. Mergia, S. Merriman, Ph. Mertens, S. Meshchaninov, A. Messiaen, R. Michling, P. Middleton, D. Middleton-Gear, J. Mietelski, D. Milanesio, E. Milani, F. Militello, A.Militello Asp, J. Milnes, A. Milocco, G. Miloshevsky, C. Minghao, S. Minucci, I. Miron, M. Miyamoto, J. Mlyn`a`r, V. Moiseenko, P. Monaghan, I. Monakhov, T. Moody, S. Moon, R. Mooney, S. Moradi, J. Morales, R.B. Morales, S. Mordijck, L. Moreira, L. Morgan, F. Moro, J. Morris, K.-M. Morrison, L. Msero, D. Moulton, T. Mrowetz, T. Mundy, M. Muraglia, A. Murari, A. Muraro, N. Muthusonai, B. N`Konga, Yong-Su Na, F. Nabais, M. Naden, J. Naish, R. Naish, F. Napoli, E. Nardon, V. Naulin, M.F.F. Nave, I. Nedzelskiy, G. Nemtsev, V. Nesenevich, I. Nestoras, R. Neu, V.S. Neverov, S. Ng, M. Nicassio, A.H. Nielsen, D. Nina, D. Nishijima, C. Noble, C.R. Nobs, M. Nocente,

D. Nodwell, K. Nordlund, H. Nordman, R. Normanton, J.M. Noterdaeme, S. Nowak, E. Nunn, H. Nyström, M. Oberparleiter, B. Obryk, J. O'Callaghan, T. Odupitan, H.J.C. Oliver, R. Olney, M. O'Mullane, J. Ongena, E. Organ, F. Orsitto, J. Orszagh, T. Osborne, R. Otin, T. Otsuka, A. Owen, Y. Oya, M. Oyaizu, R. Paccagnella, N. Pace, L.W. Packer, S. Paige, E. Pajuste, D. Palade, S.J.P. Pamela, N. Panadero, E. Panontin, A. Papadopoulos, G. Papp, P. Papp, V.V. Parail, C. Pardanaud, J. Parisi, F. Parra Diaz, A. Parsloe, M. Parsons, N. Parsons, M. Passeri, A. Patel, A. Pau, G. Pautasso, R. Pavlichenko, A. Pavone, E. Pawelec, C. Paz Soldan, A. Peacock, M. Pearce, E. Peluso, C. Penot, K. Pepperell, R. Pereira, T. Pereira, E. Perelli Cippo, P. Pereslavitsev, C. Perez von Thun, V. Pericoli, D. Perry, M. Peterka, P. Petersson, G. Petravich, N. Petrella, M. Peyman, M. Pillon, S. Pinches, G. Pintsuk, W. Pires de Sá, A. Pires dos Reis, C. Piron, L. Pionr, A. Pironti, R. Pitts, K.L. van de Plassche, N. Platt, V. Plyusnin, M. Podesta, G. Pokol, F.M. Poli, O.G. Pompilian, S. Popovichev, M. Poradzin'ski, M.T. Porfiri, M. Porkolab, C. Porosnicu, M. Porton, G. Poulipoulis, I. Predebon, G. Prestopino, C. Price, D. Price, M. Price, D. Primetzhofer, P. Prior, G. Provas, G. Pucella, P. Puglia, K. Purahoo, I. Pusztai, O. Putignano, T. Pu'tterich, A. Quercia, E. Rachlew, G. Radulescu, V. Radulovic, M. Rainford, P. Raj, G. Ralph, G. Ramogida, D. Rasmussen, J.J. Rasmussen, G. Ratt'a, S. Ratynskaia, M. Rebai, D. Réfy, R. Reichle, M. Reinke, D. Reiser, C. Reux, S. Reynolds, M.L. Richiusa, S. Richyal, D. Rigamonti, F.G. Rimini, J. Risner, M. Riva, J. Rivero-Rodriguez, C.M. Roach, R. Robins, S. Robinson, D. Robson, R. Rodionov, P. Rodrigues, M. Rodriguez Ramos, P. Rodriguez-Fernandez, F. Romanelli, M. Romanelli, S. Romanelli, J. Romazanov, R. Rossi, S. Rowe, D. Rowlands, M. Rubel, G. Rubinacci, G. Rubino, L. Ruchko, M. Ruiz, J. Ruiz Ruiz, C. Ruset, J. Rzakiewicz, S. Saarelma, E. Safi, A. Sahlberg, M. Salewski, A. Salmi, R. Salmon, F. Salzedas, I. Sanders, D. Sandiford, B. Santos, A. Santucci, K. S'arkim'aki, R. Sarwar, I. Sarychev, O. Sauter, P. Sauwan, N. Scapin, F. Schluck, K. Schmid, S. Schmuck, M. Schneider, P.A. Schneider, D. Schw'orer, G. Scott, M. Scott, D. Scraggs, S. Scully, M. Segato, Jaemin Seo, G. Sergienko, M. Sertoli, S.E. Sharapov, A. Shaw, H. Sheikh, U. Sheikh, A. Shepherd, A. Shevelev, P. Shigin, K. Shinohara, S. Shiraiwa, D. Shiraki, M. Short, G. Sias, S.A. Silburn, A. Silva, C. Silva, J. Silva, D. Silvagni, D. Simfukwe, J. Simpson, D. Sinclair, S.K. Sipil'a, A.C.C. Sips, P. Sir'en, A. Sirinelli, H. Sjöstrand, N. Skinner, J. Slater, N. Smith, P. Smith, J. Snell, G. Snoep, L. Snoj, P. Snyder, S. Soare, E.R. Solano, V. Solokha, A. Somers, C. Sommariva, K. Soni, E. Sorokovoy, M. Sos, J. Sousa, C. Sozzi, S. Spagnolo, T. Spelzini, F. Spineanu, D. Spong, D. Sprada, S. Sridhar, C. Srinivasan, G. Stables, G. Staebler, I. Stamatelatos, Z. Stancar, P. Staniec, G. Stanku'nas, M. Stead, E. Stefanikova, A. Stephen, J. Stephens, P. Stevenson, M. Stojanov, P. Strand, H.R. Strauss, S. Strikwerda, P. Str'om, C.I. Stuart, W. Studholme, M. Subramani, E. Suchkov, S. Sumida, H.J. Sun, T.E. Susti, J. Svensson, J. Svoboda, R. Sweeney, D. Sytnykov, T. Szabolics, G. Szepesi, B. Tabia, T. Tadi'c, B. T'al, T. Tala, A. Tallargio, P. Tamain, H. Tan, K. Tanaka, W. Tang, M. Tardocchi, D. Taylor, A.S. Teimane, G. Telesca, N. Teplova, A. Teplukhina, D. Terentyev, A. Terra, D. Terranova, N. Terranova, D. Testa, E. Tholerus, J. Thomas, E. Thoren, A. Thorman, W. Tierens, R.A. Tinguely, A. Tipton, H. Todd, M. Tokitani, P. Talias, M. Tome's, A. Tookey, Y. Torikai, U. von Toussaint, P. Tsavalas, D. Tskhakaya, I. Turner, M. Turner, M.M. Turner, M. Turnyanskiy, G. Tvalashvili, S. Tyrrell, M. Tyshchenko, A. Uccello, V. Udintsev, G. Urbanczyk, A. Vadgama, D. Valcarcel, M. Valisa, P. Vallejos Olivares, O. Vallhagen, M. Valovi'c, D. Van Eester, J. Varje, S. Vartanian, T. Vasilopoulou, G. Vayakis, M. Vecsei, J. Vega, S. Ventre, G. Verdoolaege, C. Verona, G. Verona Rinati, E. Veshchev, N. Vianello, E. Viezzer, L. Vignitchouk, R. Vila, R. Villari, F. Villone, P. Vincenzi, I. Vinyar, B. Viola, A.J. Virtanen, A. Vitins, Z. Vizvary, G. Vlad, M. Vlad, P. Vondr'a'cek, P. de Vries, B. Wakeling, N.R. Walkden, M. Walker, R. Walker, M. Walsh, E. Wang, N. Wang, S. Warder, R. Warren, J. Waterhouse, C. Watts, T. Wauters, A. Weckmann, H. Wedderburn Maxwell, M. Weiland, H. Weisen, M. Weiszflog, P. Welch, N. Wendler, A. West, M. Wheatley, S. Wheeler, A. Whitehead, D. Whittaker, A. Widdowson, S. Wiesen, J. Wilkinson, J.C. Williams, D. Willoughby, I. Wilson, J. Wilson, T. Wilson, M. Wischmeier, P. Wise, G. Withenshaw, A. Withycombe, D. Witts, A. Wojcik-Gargula, E. Wolfrum, R. Wood, C. Woodley, R. Woodley, B. Woods, J. Wright, J.C. Wright, T. Xu, D. Yadikin, M. Yajima, Y. Yakovenko, Y. Yang, W. Yanling, V. Yanovskiy, I. Young, R. Young, R.J. Zablockis, J. Zacks, R. Zagorski, F.S. Zaitsev, L. Zakharov, A. Zarins, D. Zarzoso Fernandez, K.-D. Zastrow, Y. Zayachuk, M. Zerbini, W. Zhang, Y. Zhou, M. Zlobinski, A. Zocco, A. Zohar, V. Zoita, S. Zoletnik, V.K. Zotta, I. Zoulias, W. Zwingmann, and I. Zychor. Overview of jet results for optimising iter operation. *Nuclear Fusion*, 62(4):

042026, jun 2022. doi: 10.1088/1741-4326/ac47b4. URL <https://dx.doi.org/10.1088/1741-4326/ac47b4>.

- [18] C. F. Maggi et al. Overview of t and d-t results in jet with iter-like wall. *to be published in Nuclear Fusion Special Issue: Overview and Summary Papers from the 29th Fusion Energy Conference (London, UK, 16-21 October 2023)*, 2023.
- [19] M. Maslov et al. Jet d-t scenario with optimized non-thermal fusion. *accepted in Nuclear Fusion*, 2023.
- [20] ITER Physics Expert Group on Confin Transport, ITER Physics Expert Group on Confin Database, and ITER Physics Basis Editors. Chapter 2: Plasma confinement and transport. *Nuclear Fusion*, 39(12):2175–2249, dec 1999. doi: 10.1088/0029-5515/39/12/302. URL <https://doi.org/10.1088%2F0029-5515%2F39%2F12%2F302>.
- [21] A.R. Polevoi, A. Loarte, N.N. Gorelenkov, Y. Gribov, S.Yu. Medvedev, R. Bilato, M. Dubrov, M. Hosokawa, A. Kavin, Ye.O. Kazakov, R. Khayrutdinov, S.H. Kim, A.Yu. Kuyanov, V. Lukash, and M. Schneider. Pfpo plasma scenarios for exploration of long pulse operation in iter. *Nuclear Fusion*, 63(7):076003, may 2023. doi: 10.1088/1741-4326/acd06f. URL <https://dx.doi.org/10.1088/1741-4326/acd06f>.
- [22] R. J. Hawryluk. An empirical approach to tokamak transport. In *Physics of plasmas close to thermonuclear conditions*, pages 19–46. Elsevier, 1981.
- [23] C. Angioni, P. Mantica, T. Pütterich, M. Valisa, M. Baruzzo, E.A. Belli, P. Belo, F.J. Casson, C. Challis, P. Drewelow, C. Giroud, N. Hawkes, T.C. Hender, J. Hobirk, T. Koskela, L. Lauro Taroni, C.F. Maggi, J. Mlynar, T. Odstrcil, M.L. Reinke, and M. Romanelli. Tungsten transport in JET h-mode plasmas in hybrid scenario, experimental observations and modelling. *Nuclear Fusion*, 54(8):083028, jul 2014. doi: 10.1088/0029-5515/54/8/083028.
- [24] C. Z. Cheng, L. Chen, and M. S. Chance. High-n ideal and resistive shear Alfvén waves in tokamaks. *Annals of Physics*, 161(1):21–47, 1985.
- [25] C. Z. Cheng and M. S. Chance. Low-n shear Alfvén spectra in axisymmetric toroidal plasmas. *Physics of Fluids*, 29:3695, 1986.
- [26] S. E. Sharapov, B. Alper, H. L. Berk, D. N. Borba, B. N. Breizman, C. D. Challis, A. Fasoli, N. C. Hawkes, T. C. Hender, J. Mailloux, S. D. Pinches, D. Testa, and EFDA–JET work programme. Alfvén wave cascades in a tokamak. *Physics of Plasmas*, 9(5):2027–2036, 04 2002. ISSN 1070-664X. doi: 10.1063/1.1448346. URL <https://doi.org/10.1063/1.1448346>.
- [27] Liu Chen, R. B. White, and M. N. Rosenbluth. Excitation of internal kink modes by trapped energetic beam ions. *Phys. Rev. Lett.*, 52:1122–1125, Mar 1984. doi: 10.1103/PhysRevLett.52.1122. URL <https://link.aps.org/doi/10.1103/PhysRevLett.52.1122>.
- [28] B. Coppi and F. Porcelli. Theoretical model of fishbone oscillations in magnetically confined plasmas. *Phys. Rev. Lett.*, 57:2272–2275, Nov 1986. doi: 10.1103/PhysRevLett.57.2272. URL <https://link.aps.org/doi/10.1103/PhysRevLett.57.2272>.
- [29] Z. Chang, J. D. Callen, E. D. Fredrickson, R. V. Budny, C. C. Hegna, K. M. McGuire, M. C. Zarnstorff, and TFTR group. Observation of nonlinear neoclassical pressure-gradient-driven tearing modes in tftr. *Phys. Rev. Lett.*, 74:4663–4666, Jun 1995. doi: 10.1103/PhysRevLett.74.4663. URL <https://link.aps.org/doi/10.1103/PhysRevLett.74.4663>.
- [30] O. Sauter, R. J. La Haye, Z. Chang, D. A. Gates, Y. Kamada, H. Zohm, A. Bondeson, D. Boucher, J. D. Callen, M. S. Chu, T. A. Gianakon, O. Gruber, R. W. Harvey, C. C. Hegna, L. L. Lao, D. A. Monticello, F. Perkins, A. Pletzer, A. H. Reiman, M. Rosenbluth, E. J. Strait, T. S. Taylor, A. D. Turnbull, F. Waelbroeck, J. C. Wesley, H. R. Wilson, and R. Yoshino. Beta limits in long-pulse tokamak discharges. *Physics of Plasmas*, 4(5): 1654–1664, 05 1997. ISSN 1070-664X. doi: 10.1063/1.872270. URL <https://doi.org/10.1063/1.872270>.
- [31] F Romanelli. Ion temperature-gradient-driven modes and anomalous ion transport in tokamaks. *Physics of Fluids B: Plasma Physics*, 1(5):1018–1025, 1989.
- [32] S. Mazzi, J. Garcia, D. Zarzoso, Ye. O. Kazakov, J. Ongena, M. Dreval, M. Nocente, Ž. Stancar, G. Szepesi, J. Eriksson, A. Sahlberg, S. Benkadda, N. Abid, K. Abraham, P. Abreu, O. Adabonyan, P. Adrich, M. Afzal, T. Ahlgren, L. Aho-Mantila, N. Aiba, M. Airila, M. Akhtar, R. Albanese, M. Alderson-Martin, D. Alegre, S. Aleiferis, A. Aleksa, E. Alessi, P. Aleynikov, J. Alguacil, M. Ali, M. Allinson, B. Alper, E. Alves, G. Ambrosino, R. Ambrosino, E. Andersson Sundén, P. Andrew, B. M. Angelini, C. Angioni, I. Antoniou,

L. C. Appel, C. Appelbee, S. Aria, M. Ariola, G. Artaserse, W. Arter, V. Artigues, N. Asakura, A. Ash, N. Ashikawa, V. Aslanyan, M. Astrain, O. Asztalos, D. Auld, F. Auriemma, Y. Austin, L. Avotina, E. Aymerich, A. Baciero, F. Bairaktaris, J. Balbin, L. Balbinot, I. Balboa, M. Balden, C. Balshaw, N. Balshaw, V. K. Bandaru, J. Banks, Yu. F. Baranov, C. Barcellona, A. Barnard, M. Barnard, R. Barnsley, A. Barth, M. Baruzzo, S. Barwell, M. Bassan, A. Batista, P. Batistoni, L. Baumane, B. Bauvir, L. Baylor, P. S. Beaumont, D. Beckett, A. Begolli, M. Beidler, N. Bekris, M. Beldishevski, E. Belli, F. Belli, E. Belonohy, M. Ben Yaala, J. Benayas, J. Bentley, H. Bergsaker, J. Bernardo, M. Bernert, M. Berry, L. Bertalot, H. Betar, M. Beurskens, S. Bickerton, B. Bieg, J. Bielecki, A. Bierwage, T. Biewer, R. Bilato, P. Bilkov'a, G. Birkenmeier, H. Bishop, J. P. S. Bizarro, J. Blackburn, P. Blanchard, P. Blatchford, V. Bobkov, A. Boboc, P. Bohm, T. Bohm, I. Bolshakova, T. Bolzonella, N. Bonanomi, D. Bonfiglio, X. Bonnin, P. Bonofiglio, S. Boocock, A. Booth, J. Booth, D. Borba, D. Borodin, I. Borodkina, C. Boulbe, C. Bourdelle, M. Bowden, K. Boyd, I. Božičević Mihalić, S. C. Bradnam, V. Braic, L. Brandt, R. Bravanec, B. Breizman, A. Brett, S. Brezinsek, M. Brix, K. Bromley, B. Brown, D. Brunetti, R. Buckingham, M. Buckley, R. Budny, J. Buermans, H. Bufferand, P. Buratti, A. Burgess, A. Buscarino, A. Busse, D. Butcher, E. de la Cal, G. Calabrò, L. Calacci, R. Calado, Y. Camenen, G. Canal, B. Cannas, M. Cappelli, S. Carcangiu, P. Card, A. Cardinali, P. Carman, D. Carnevale, M. Carr, D. Carralero, L. Carraro, I. S. Carvalho, P. Carvalho, I. Casiraghi, F. J. Casson, C. Castaldo, J. P. Catalan, N. Catarino, F. Causa, M. Cavedon, M. Cecconello, C. D. Challis, B. Chamberlain, C. S. Chang, A. Chankin, B. Chapman, M. Chernyshova, A. Chiariello, P. Chmielewski, A. Chomiczewska, L. Chone, G. Ciraolo, D. Ciric, J. Citrin, L. Ciupinski, M. Clark, R. Clarkson, C. Clements, M. Cleverly, J. P. Coad, P. Coates, A. Cobalt, V. Coccoresse, R. Coelho, J. W. Coenen, I. H. Coffey, A. Colangeli, L. Colas, C. Collins, J. Collins, S. Collins, D. Conka, S. Conroy, B. Conway, N. J. Conway, D. Coombs, P. Cooper, S. Cooper, C. Corradino, G. Corrigan, D. Coster, P. Cox, T. Craciunescu, S. Cramp, C. Crapper, D. Craven, R. Craven, M. Crialesi Esposito, G. Croci, D. Croft, A. Croitoru, K. Cromb'e, T. Cronin, N. Cruz, C. Crystal, G. Cseh, A. Cufar, A. Cullen, M. Curuia, T. Czarski, H. Dabirikhah, A. Dal Molin, E. Dale, P. Dalgliesh, S. Dalley, J. Dankowski, P. David, A. Davies, S. Davies, G. Davis, K. Dawson, S. Dawson, I. E. Day, M. De Bock, G. De Temmerman, G. De Tommasi, K. Deakin, J. Deane, R. Dejarnac, D. Del Sarto, E. Delabie, D. Del-Castillo-Negrete, A. Dempsey, R. O. Dendy, P. Devynck, A. Di Siena, C. Di Troia, T. Dickson, P. Dinca, T. Dittmar, J. Dobrashian, R. P. Doerner, A. J. H. Donn'e, S. Dorling, S. Dormido-Canto, D. Douai, S. Dowson, R. Doyle, P. Drewelow, P. Drews, G. Drummond, Ph. Duckworth, H. Dudding, R. Dumont, P. Dumortier, D. Dunai, T. Dunatov, M. Dunne, I. Duran, F. Durodi'e, R. Dux, A. Dvornova, R. Eastham, J. Edwards, Th. Eich, and J. E. T. Contributors. Enhanced performance in fusion plasmas through turbulence suppression by megaelectronvolt ions. *Nature Physics*, 18(7):776–782, Jul 2022. ISSN 1745-2481. doi: 10.1038/s41567-022-01626-8. URL <https://doi.org/10.1038/s41567-022-01626-8>.

- [33] P. Mantica, N. Bonanomi, A. Mariani, P. Carvalho, E. Delabie, J. Garcia, N. Hawkes, T. Johnson, D. Keeling, M. Sertoli, G.M. Staebler, G. Szepesi, D. Taylor, A. Thorman, and JET Contributors. The role of electronscale turbulence in the jet tokamak: experiments and modelling. *Nuclear Fusion*, 61(9):096014, aug 2021. doi: 10.1088/1741-4326/ac146e. URL <https://dx.doi.org/10.1088/1741-4326/ac146e>.
- [34] S. Elgar and R.T. Guza. Statistics of bicoherence. *IEEE Transactions on Acoustics, Speech, and Signal Processing*, 36(10):1667–1668, 1988. doi: 10.1109/29.7555.
- [35] S. Hacquin, S. E. Sharapov, B. Alper, C. D. Challis, A. Fonseca, E. Mazzucato, A. Meigs, L. Meneses, I. Nunes, S. D. Pinches, et al. Localized X-mode reflectometry measurements of Alfvén eigenmodes on the JET tokamak. *Plasma Physics and Controlled Fusion*, 49(9):1371, 2007.
- [36] D.A. Spong, M.A. Van Zeeland, W.W. Heidbrink, X. Du, J. Varela, L. Garcia, and Y. Ghai. Nonlinear dynamics and transport driven by energetic particle instabilities using a gyro-landau closure model*. *Nuclear Fusion*, 61(11):116061, oct 2021. doi: 10.1088/1741-4326/ac2990. URL <https://dx.doi.org/10.1088/1741-4326/ac2990>.
- [37] P. J. Bonofiglio, V. Kiptily, A. Horton, P. Beaumont, R. Ellis, F. E. Cecil, M. Podesta, and JET Contributors. Improvements to the Faraday cup fast ion loss detector and magnetohydrodynamic induced fast ion loss measurements in Joint European Torus plasmas. *Review of Scientific Instruments*, 91(9):093502, 09 2020. ISSN 0034-6748. doi: 10.1063/5.0014278. URL <https://doi.org/10.1063/5.0014278>.

- [38] Liu Chen and Fulvio Zonca. Nonlinear excitations of zonal structures by toroidal Alfvén eigenmodes. *Phys. Rev. Lett.*, 109:145002, Oct 2012. doi: 10.1103/PhysRevLett.109.145002. URL <https://link.aps.org/doi/10.1103/PhysRevLett.109.145002>.
- [39] A Mishchenko, A Biancalani, M Borchardt, A Bottino, S Briguglio, R Dumont, J Ferreira, J P Graves, T Hayward-Schneider, R Kleiber, A Kˆonies, E Lanti, Ph Lauber, H Leyh, Z X Lu, H Lutjens, B McMillan, M Campos Pinto, E Poli, B Rettino, B Rofman, J N Sama, C Slaby, F Vannini, L Villard, G Vlad, X Wang, F Widmer, and F Zonca. Numerical tools for burning plasmas. *Plasma Physics and Controlled Fusion*, 65(6): 064001, apr 2023. doi: 10.1088/1361-6587/acce68. URL <https://dx.doi.org/10.1088/1361-6587/acce68>.
- [40] A. Di Siena, T. Gˆorler, H. Doerk, E. Poli, and R. Bilato. Fast-ion stabilization of tokamak plasma turbulence. *Nuclear Fusion*, 58(5):054002, 2018.
- [41] P. H. Diamond, S. I. Itoh, K. Itoh, and T. S. Hahm. Zonal flows in plasmas - a review. *Plasma Physics and Controlled Fusion*, 47:R35, 2005.
- [42] J Garcia and JET Contributors. Electromagnetic and fast ions effects as a key mechanism for turbulent transport suppression at jet. *Plasma Physics and Controlled Fusion*, 64(10):104002, aug 2022. doi: 10.1088/1361-6587/ac8613. URL <https://dx.doi.org/10.1088/1361-6587/ac8613>.
- [43] J. Candy, E.A. Belli, and R.V. Bravenec. A high-accuracy eulerian gyrokinetic solver for collisional plasmas. *Journal of Computational Physics*, 324:73–93, 2016. ISSN 0021-9991. doi: <https://doi.org/10.1016/j.jcp.2016.07.039>. URL <https://www.sciencedirect.com/science/article/pii/S0021999116303400>.
- [44] H. Sugama and W. Horton. Nonlinear electromagnetic gyrokinetic equation for plasmas with large mean flows. *Physics of Plasmas*, 5(7):2560–2573, 07 1998. ISSN 1070-664X. doi: 10.1063/1.872941. URL <https://doi.org/10.1063/1.872941>.
- [45] D. Kim, S.J. Park, G.J. Choi, Y.W. Cho, J. Kang, H. Han, J. Candy, E.A. Belli, T.S. Hahm, Y.-S. Na, and C. Sung. Turbulence stabilization in tokamak plasmas with high population of fast ions. *Nuclear Fusion*, 63(12): 124001, oct 2023. doi: 10.1088/1741-4326/acffda. URL <https://dx.doi.org/10.1088/1741-4326/acffda>.
- [46] J. Garcia, T. Gorler, F. Jenko, and G. Giruzzi. Gyrokinetic nonlinear isotope effects in tokamak plasmas. *Nuclear Fusion*, 57(1):014007, dec 2016. doi: 10.1088/1741-4326/57/1/014007. URL <https://doi.org/10.1088/1741-4326/57/1/014007>.
- [47] J. Garcia, T. Gorler, and F. Jenko. Isotope and fast ions turbulence suppression effects: Consequences for high- β ITER plasmas. *Physics of Plasmas*, 25(5):055902, 2018.
- [48] E. A. Belli, J. Candy, and R. E. Waltz. Reversal of simple hydrogenic isotope scaling laws in tokamak edge turbulence. *Phys. Rev. Lett.*, 125:015001, Jun 2020. doi: 10.1103/PhysRevLett.125.015001. URL <https://link.aps.org/doi/10.1103/PhysRevLett.125.015001>.
- [49] C F Maggi, H Weisen, J C Hillesheim, A Chankin, E Delabie, L Horvath, F Auriemma, I S Carvalho, G Corrigan, J Flanagan, L Garzotti, D Keeling, D King, E Lerche, R Lorenzini, M Maslov, S Menmuir, S Saarelma, A C C Sips, E R Solano, E Belonohy, F J Casson, C Challis, C Giroud, V Parail, C Silva, M Valisa, and JET Contributors. Isotope effects on I-h threshold and confinement in tokamak plasmas. *Plasma Physics and Controlled Fusion*, 60(1):014045, nov 2017. doi: 10.1088/1361-6587/aa9901. URL <https://dx.doi.org/10.1088/1361-6587/aa9901>.
- [50] L. Frassinetti et al. Effect of the isotope mass on pedestal structure, transport and stability in d, dt and t plasmas at constant betan and gas rate in jet-ilw. *Nucl. Fusion Special Issue on JET T and D-T, 2023*, 2023.
- [51] P. Schneider et al. Isotope physics of heat and particle transport with tritium in jet-ilw type-i elmy h-mode. *Nucl. Fusion Special Issue on JET T and D-T, 2023*, 2023.
- [52] L. Horvath, C.F. Maggi, A. Chankin, S. Saarelma, A.R. Field, S. Aleiferis, E. Belonohy, A. Boboc, G. Corrigan, E.G. Delabie, J. Flanagan, L. Frassinetti, C. Giroud, D. Harting, D. Keeling, D. King, M. Maslov, G.F. Matthews, S. Menmuir, S.A. Silburn, J. Simpson, A.C.C. Sips, H. Weisen, K.J. Gibson, and JET Contributors. Isotope dependence of the type i ELMY h-mode

pedestal in JET-ILW hydrogen and deuterium plasmas. *Nuclear Fusion*, 61(4):046015, mar 2021. doi: 10.1088/1741-4326/abdd77. URL <https://doi.org/10.1088/1741-4326/abdd77>.

- [53] Emilia R. Solano, N. Vianello, E. Delabie, J.C. Hillesheim, P. Buratti, D. R'efy, I. Balboa, A. Boboc, R. Coelho, B. Sieglin, S. Silburn, P. Drewelow, S. Devaux, D. Dodt, A. Figueiredo, L. Frassinetti, S. Marsen, L. Meneses, C.F. Maggi, J. Morris, S. Gerasimov, M. Baruzzo, M. Stamp, D. Grist, I. Nunes, F. Rimini, S. Schmuck, I. Lupelli, C. Silva, and JET contributors. Axisymmetric oscillations at I-h transitions in jet: M-mode. *Nuclear Fusion*, 57(2):022021, oct 2016. doi: 10.1088/0029-5515/57/2/022021. URL <https://dx.doi.org/10.1088/0029-5515/57/2/022021>.
- [54] E. Delabie, J. C. Hillesheim, J. Mailloux, C. Maggi, F. Rimini, and E. Solano. The low density type iii elmy h-mode regime on jet-ilw: a low density h-mode compatible with a tungsten divertor?. *BP10.00052, 58th Annual Meeting of the APS Division of Plasma Physics, October 31–November 4 2016, San Jose, California*, 2016.
- [55] F Ryter, W Suttrop, B Bru¨sehaber, M Kaufmann, V Mertens, H Murmann, A G Peeters, J Stober, J Schweinzer, H Zohm, and ASDEX Upgrade Team. H-mode power threshold and transition in asdex upgrade. *Plasma Physics and Controlled Fusion*, 40(5):725, may 1998. doi: 10.1088/0741-3335/40/5/032. URL <https://dx.doi.org/10.1088/0741-3335/40/5/032>.
- [56] M Greenwald, J Schachter, W Dorland, R Granetz, A Hubbard, J Rice, J A Snipes, P Stek, and S Wolfe. Transport phenomena in alcator c-mod h-modes. *Plasma Physics and Controlled Fusion*, 40(5):789, may 1998. doi: 10.1088/0741-3335/40/5/044. URL <https://dx.doi.org/10.1088/0741-3335/40/5/044>.
- [57] D.G. Whyte, A.E. Hubbard, J.W. Hughes, B. Lipschultz, J.E. Rice, E.S. Marmar, M. Greenwald, I. Cziegler, A. Dominguez, T. Golfopoulos, N. Howard, L. Lin, R.M. McDermott, M. Porkolab, M.L. Reinke, J. Terry, N. Tsujii, S. Wolfe, S. Wukitch, Y. Lin, and the Alcator C-Mod Team. I-mode: an h-mode energy confinement regime with I-mode particle transport in alcator c-mod. *Nuclear Fusion*, 50(10):105005, oct 2010. doi: 10.1088/0029-5515/50/10/105005. URL <https://dx.doi.org/10.1088/0029-5515/50/10/105005>.
- [58] M. Shimada et al. Chapter 1: Overview and summary. *Nuclear Fusion*, 47:S1–S17, 2007.
- [59] A. J. Creely, M. J. Greenwald, S. B. Ballinger, D. Brunner, J. Canik, J. Doody, T. Fu¨ll´op, D. T. Garnier, R. Granetz, T. K. Gray, and et al. Overview of the sparc tokamak. *Journal of Plasma Physics*, 86(5): 865860502, 2020. doi: 10.1017/S0022377820001257.
- [60] N. C. Hawkes, E. Delabie, S. Menmuir, C. Giroud, A. G. Meigs, N. J. Conway, T. M. Biewer, D. L. Hillis, and JET Contributors. Instrumentation for the upgrade to the JET core charge-exchange spectrometers. *Review of Scientific Instruments*, 89(10):10D113, 08 2018. ISSN 0034-6748. doi: 10.1063/1.5037639. URL <https://doi.org/10.1063/1.5037639>.
- [61] M Maslov, M N A Beurskens, M Kempnaars, and J Flanagan. Status of the jet lidar thomson scattering diagnostic. *Journal of Instrumentation*, 8(11):C11009, nov 2013. doi: 10.1088/1748-0221/8/11/C11009. URL <https://dx.doi.org/10.1088/1748-0221/8/11/C11009>.
- [62] R. Pasqualotto, P. Nielsen, C. Gowers, M. Beurskens, M. Kempnaars, T. Carlstrom, D. Johnson, and JETEFDA Contributors. High resolution Thomson scattering for Joint European Torus (JET). *Review of Scientific Instruments*, 75(10):3891–3893, 10 2004. ISSN 0034-6748. doi: 10.1063/1.1787922. URL <https://doi.org/10.1063/1.1787922>.
- [63] R.A. Tinguely, J. Gonzalez-Martin, P.G. Puglia, N. Fil, S. Dowson, M. Porkolab, I. Kumar, M. Podesta, M. Baruzzo, A. Fasoli, Ye.O. Kazakov, M.F.F. Nave, M. Nocente, J. Ongena, Z.Stancar, and JET Contributors. Simultaneous measurements of unstable and stable Alfvén eigenmodes in jet. *Nuclear Fusion*, 62(11):112008, sep 2022. doi: 10.1088/1741-4326/ac899e. URL <https://dx.doi.org/10.1088/1741-4326/ac899e>.
- [64] M. Maslov, D.B. King, E. Viezzer, D.L. Keeling, C. Giroud, T. Tala, A. Salmi, M. Marin, J. Citrin, C. Bourdelle, and E.R. Solano and. Observation of enhanced ion particle transport in mixed h/d isotope plasmas on JET. *Nuclear Fusion*, 58(7):076022, jun 2018. doi: 10.1088/1741-4326/aac342. URL <https://doi.org/10.1088/1741-4326/aac342>.
- [65] J. Ongena, I. Voitsekhovitch, M. Evrard, and D. McCune. Numerical Transport Codes. *Fusion Science and Technology*, 61(2T):180–189, 2012. doi: 10.13182/FST12-A13505. URL <https://doi.org/10.13182/FST12-A13505>.

- [66] A. Pankin, D. McCune, R. Andre, G. Bateman, and A. Kritz. The tokamak Monte Carlo fast ion module NUBEAM in the National Transport Code Collaboration library. *Computer Physics Communications*, 159(3): 157–184, 2004.
- [67] M. Brambilla. Numerical simulation of ion cyclotron waves in tokamak plasmas. *Plasma Physics and Controlled Fusion*, 41(1):1, 1999.
- [68] B. A. Grierson, X. Yuan, M. Gorelenkova, S. Kaye, N. C. Logan, O. Meneghini, S. R. Haskey, J. Buchanan, M. Fitzgerald, S. P. Smith, et al. Orchestrating TRANSP simulations for interpretative and predictive tokamak modeling with OMFIT. *Fusion Science and Technology*, 74(1-2):101–115, 2018.
- [69] C. L. Hedrick, J.-N. Leboeuf, and D. A. Spong. Alpha-Alfvén local dispersion relation and solutions. *Physics of Fluids B: Plasma Physics*, 4(12):3869–3882, 12 1992. ISSN 0899-8221. doi: 10.1063/1.860344. URL <https://doi.org/10.1063/1.860344>.
- [70] D. A. Spong, B. A. Carreras, and C. L. Hedrick. Linearized gyrofluid model of the alpha-destabilized toroidal Alfvén eigenmode with continuum damping effects. *Physics of Fluids B: Plasma Physics*, 4(10):3316–3328, 10 1992. ISSN 0899-8221. doi: 10.1063/1.860386. URL <https://doi.org/10.1063/1.860386>.
- [71] J. Varela, A. Shimizu, D.A. Spong, L. Garcia, and Y. Ghai. Study of the alfvén eigenmodes stability in cfqs plasma using a landau closure model. *Nuclear Fusion*, 61(2):026023, jan 2021. doi: 10.1088/1741-4326/abd072. URL <https://dx.doi.org/10.1088/1741-4326/abd072>.
- [72] J. Varela, D.A. Spong, L. Garcia, S. Ohdachi, K.Y. Watanabe, R. Seki, and Y. Ghai. Theoretical analysis of the saturation phase of the 1/1 energetic-ion-driven resistive interchange mode. *Nuclear Fusion*, 61(12): 126016, oct 2021. doi: 10.1088/1741-4326/ac26a0. URL <https://dx.doi.org/10.1088/1741-4326/ac26a0>.
- [73] S. P. Hirshman and J. C. Whitson. Steepest-descent moment method for three-dimensional magnetohydrodynamic equilibria. *The Physics of Fluids*, 26(12):3553–3568, 12 1983. ISSN 0031-9171. doi: 10.1063/1.864116. URL <https://doi.org/10.1063/1.864116>.
- [74] H. Sugama, T.-H. Watanabe, and M. Nunami. Linearized model collision operators for multiple ion species plasmas and gyrokinetic entropy balance equations. *Physics of Plasmas*, 16(11):112503, 11 2009. ISSN 1070664X. doi: 10.1063/1.3257907. URL <https://doi.org/10.1063/1.3257907>.

Acknowledgments

J. Garcia would like to thank Gerardo Giruzzi for fruitful discussions.

This work has been carried out within the framework of the EUROfusion Consortium, funded by the European Union via the Euratom Research and Training Programme (Grant Agreement No 101052200 - EUROfusion) and from the EPSRC [grant number EP/W006839/1]. Views and opinions expressed are however those of the author(s) only and do not necessarily reflect those of the European Union or the European Commission. Neither the European Union nor the European Commission can be held responsible for them.

This work was partly supported by grants FIS2017-85252-R and PID2021-127727OB-I00, funded by the Spanish Ministry of Science and Innovation.

An award of computer time was provided by the INCITE program and ALCC program. This research used resources from the Oak Ridge Leadership Computing Facility, which is an Office of Science User Facility supported under Contract DE-AC05-00OR22725. Computing resources were also provided by the National Energy Research Scientific Computing Center, which is an Office of Science User Facility supported under Contract DEAC0205CH11231.

Author contributions

The reported experiments were devised and jointly led by Y.K., J.O., S.S., J.G. and M.B., with the key coordination of E. de la L., C.F.M and J.M. The TRANSP simulations were performed by Z.S. and M.P. Gyrokinetic simulations and subsequent analyses were performed by E.B, J.C. and S.M. FAR3D simulations were performed by J.V. with the assistance of D.Z. Reflectometer analyses were performed by M.D. and J.R.R. MHD analyses were performed by R.C. and M.D. Pedestal analyses were performed by E.de la L. and E.S. Alpha particle losses were investigated by P.J.B. The manuscript was written by J.G. and E. de la L. with the feedback by all the authors.

Competing interests

The authors declare no competing interests.

Additional Information

Correspondence and requests for materials should be addressed to J. Garcia.